JOURNAL OF GEOPHYSICAL RESEARCH, VOL. 111, C03S13, doi:10.1029/2005JC003377, 2006 [printed 112(C3), 2007]

Modeling the northern Adriatic double-gyre response to intense bora wind: A revisit

Milivoj Kuzmić,[1] Ivica Janeković,[1] Jeffrey W. Book,[2] Paul J. Martin,[2] and James D. Doyle[3]

Received 11 April 2006; revised 24 July 2006; accepted 12 September 2006; published 27 December 2006.

[1] A combination of recent intensive observations and simulations with two numerical models is used to revisit the issue of the northern Adriatic response to strong bora episodes. New observed and simulated data reinforce the view that an episode of strong bora wind provokes a double-gyre (cyclonic, Trieste, and anticyclonic, Rovinj) response north of the Po Delta - Pula line. During an intense bora episode, both measured and modeled statistics picture a downwind, highly polarized, and almost depth-independent flow within the Trieste gyre NW arm. Its NE arm maintains a sharp polarization and strong depth dependence while exhibiting lower speeds, with models in good accord with observations. The current statistics for Rovinj gyre provide lower maximum and average speed values and less polarized but still rather depth-independent flow, while exhibiting clockwise rotation. The north arm of the Senj gyre (positioned south of the Po Delta–Pula line) enjoys more lateral freedom, and exhibits less rectilinear flow. Our review reinforces the notion that modeling studies based on ECMWF wind forcing fail to properly take into account the orographic control of the Dinaric Alps, and to produce correct bora-induced gyral pattern. The COAMPS® model successfully simulated the onset, duration, and decay of the wind peaks, but exhibited a tendency to overpredict the strength of the bora wind. Our simulations have identified the shallow NW coastal strip as an important source of colder water observed in a sequence of remotely sensed SST fields derived from AVHRR data.

Citation: Kuzmić, M., I. Janeković, J. W. Book, P. J. Martin, and J. D. Doyle (2006), Modeling the northern Adriatic double-gyre response to intense bora wind: A revisit, *J. Geophys. Res.*, *111*, C03S13, doi:10.1029/2005JC003377. [printed *112*(C3), 2007]

1. Introduction

[2] The northern Adriatic is the northernmost part of the Mediterranean basin with the Apennines, Alps, and Dinaric Alps providing its complex orographic surroundings. One of the better known winds there is the bora, a cold, dry, and gusty downslope flow of air of prevailing northeasterly direction. The bora wind is an outcome of cold air buildup over continental Europe, lower pressure over the Adriatic Sea, and the consequent pressure gradient across the Dinaric Alps. Although the bora is closely related to mesoscale features and synoptic-scale flow interactions with the Alpine massif [*Ivančan-Picek and Tutiš*, 1996], gaps and passes in the Dinaric Alps (Figure 1) exert an important orographic control, imposing, among other effects, lateral shearing in the wind stress field. In a series of numerical experiments, *Lazić and Tošić* [1998] showed that a mountain barrier about 1000 m high is needed for the occurrence of bora-type downslope wind. Too low a barrier prevents accumulation of cold air and too high a barrier produces a blocking effect. In one of the first efforts to model the ocean response to lateral variability of the northern-Adriatic bora wind, *Stravisi* [1977] used a two-dimensional, storm-surge model, which assumed a sine-squared function for the lateral wind-stress decay. *Kuzmić and Orlić* [1987] (hereafter KO) used the ten-year statistics of *Yoshino* [1972] and *Penzar* [1977] and an interpolation scheme to synthesize a climatological, laterally variable, wind forcing field. When applied to force a three-dimensional, modal, numerical model into a frictionally controlled, quasi-steady state, it enforced a double-gyre response on the northern-Adriatic circulation northwest of the Pula-Pesaro line (Figure 1). A large cyclonic gyre was obtained covering most of the northern Adriatic, with an anticyclonic gyre apparently formed southeast of it, which was clearly contaminated by the proximity of the model open boundary. When the model was extended to cover the whole Adriatic and forced with a similarly derived wind field [*Kuzmić et al.*, 1988], the anticyclonic gyre emerged more clearly and reliably. This work was later expanded to include sirocco winds and more complete interpretation [*Orlić et al.*, 1994]. The upwind, cross-basin flow (part of the cyclonic gyre) received an empirical confirmation in a comparison with CZCS data [*Kuzmić*, 1991].

[1] Center for Marine and Environmental Research, Ruđer Bošković Institute, Zagreb, Croatia.
[2] Oceanography Division, Naval Research Laboratory, Stennis Space Center, Mississippi, USA.
[3] Marine Meteorology Division, Naval Research Laboratory, Monterey, California, USA.

0148-0227/06/2005JC003377$09.00

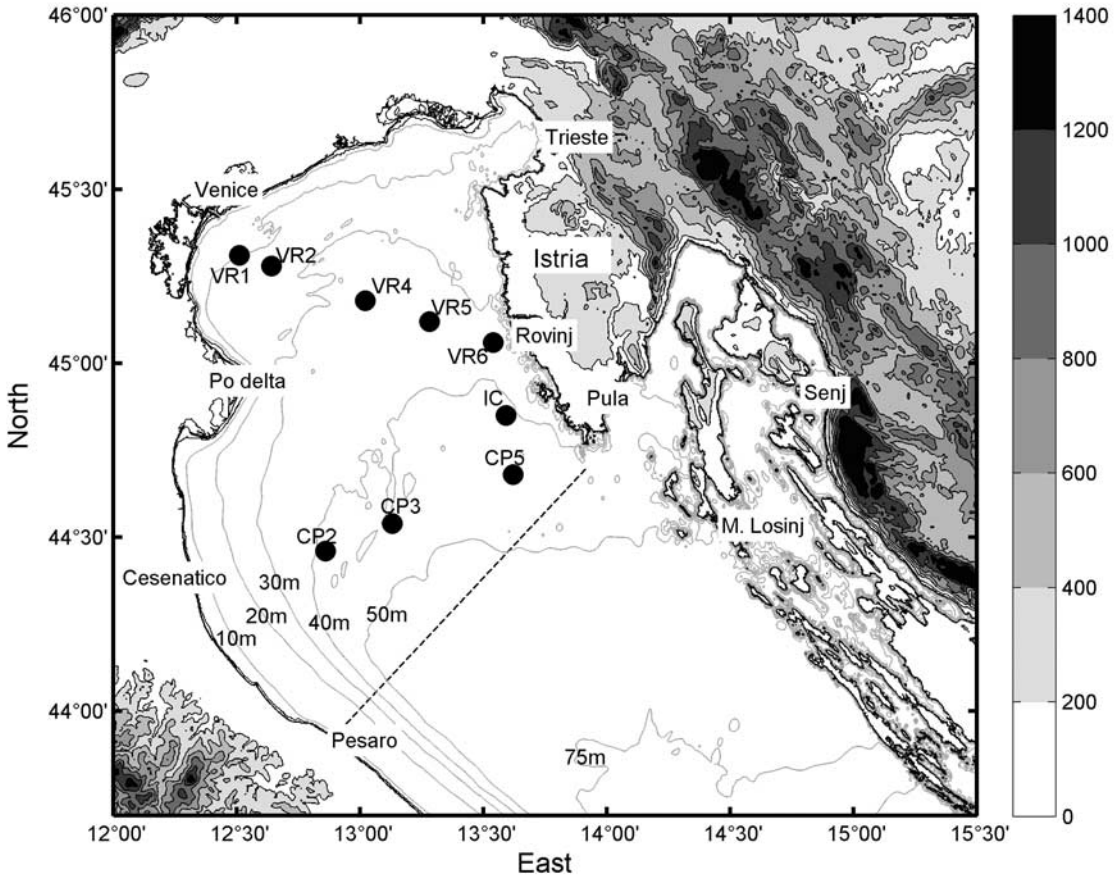

Figure 1. The northern Adriatic bathymetry (contoured, meters) and the orography of the surrounding mountains (shaded, meters). The three-character names mark the locations of the ADCP stations. Also marked are the open boundary of the KO model (dashed line) and the names of the locations mentioned in the text.

[3] In this paper, we revisit the simplistic KO simulations and reconsider them in the light of recent extensive field evidence and more powerful model results. The purpose of the revisit is threefold: (a) to review the modeling progress made since the publication of the KO paper; (b) to address the validity of the double-gyre response with state-of-the-art modeling tools; and (c) to verify the new modeling results with the currently available, much larger set of field data. The reanalysis is based on a sequence of more sophisticated atmospheric and oceanographic model simulations and is focused on the January–February 2003 bora events. A high-resolution, three-dimensional, finite-element model is used to generate a suite of simpler, exploratory simulations with a view to provide a more insightful interpretation of an all-included, long-term simulation provided by another model. In contrast to our reference work (KO) and some other studies dealing with (simplified) generic processes, seasonal variations, or dominant circulation patterns, we focus on verifiable predictions of several real bora episodes. The novel points of the revisit are the use of two, sophisticated, state-of-the-art models of different development, which have (a) more realistic physics, (b) higher-resolution computational grids, (c) hourly atmospheric forcing, which allows detailed forcing at the air-sea interface, and (d) verification based on observations from two recent field programs. The improved verification relies on extensive data sets collected at 9 (out of 18) locations over a period of 5–9 months within the framework of the Joint Research Project (JRP) (the U.S. Naval Research Laboratory (NRL) and the NATO Undersea Research Center (NURC)) and the Ruđer Bošković Institute (RBI) West IStria Experiment (WISE). The results of the field measurements in the JRP and WISE framework, together with other sources, provide an unprecedented empirical reference for validation of the studied response.

[4] Understanding of the northern Adriatic circulation, including observations and numerical simulations, at the end of past century has been synthesized in a recent monograph [*Cushman-Roisin et al.*, 2001]. After a relatively quiet period, the bora-wind-driven Adriatic Sea circulation recently received attention in several papers. *Beg Paklar et al.* [2001] performed a numerical model study of the Adriatic shelf-water response to the Po River discharge and a bora event. The study employed an MM5 prediction of the wind stress and surface heat flux to force a version of the Princeton Ocean Model (POM) set up for the Adriatic at 9-km resolution. The authors experimented with a suite of forcing combinations that pointed out the importance of proper treatment of air stability and the wind-wave field. Regardless of the treatment of these parameters, they obtained a large cyclonic gyre over most of the northern Adriatic, another large cyclonic gyre

south of it (bellow the Pula-Pesaro line, Figure 1), and an indication of anti-cyclonic motion in between.

[5] In a four-experiment numerical study, *Rachev and Purini* [2001] focused on the bora wind effects on the Adriatic Sea circulation. In these experiments, they forced an Adriatic implementation of the DieCAST ocean model at a spatial resolution of 5.3 km with an idealized wind stress field pattern based on that used by *Bergamasco and Gačić* [1996]. The authors were primarily concerned with questions of the bora contribution to the residual Adriatic circulation and the exchange at the Strait of Otranto. Their model grid resolution was sufficient to resolve details of the bora-induced circulation in the northern Adriatic; however, the schematized nature of their wind stress field allowed generation of only a partially realistic northern Adriatic gyral pattern.

[6] *Pullen et al.* [2003] performed a realistic, 125-day long simulation (28 January–4 June 2001) of the Adriatic Sea circulation with the Navy Coastal Ocean Model (NCOM) coupled to the Coupled Ocean/Atmosphere Mesoscale Prediction System (COAMPS®) with a view to identify model-derived patterns of circulation in both the sea and atmosphere. In addition to assessment of the predicted atmospheric and oceanic velocity fields, the authors set out to quantify the impact of the atmospheric model resolution on the predictive skill of the ocean model. The double-gyre circulation pattern was found to be a generic Adriatic response to the wind-stress vorticity field. The high-resolution, 4-km atmospheric forcing produced more realistic looking bora features, but low-resolution, 36-km model exhibited superior agreement with observations at two ADCP-instrumented sites for several major statistics.

[7] *Loglisci et al.* [2004] applied a two-way coupled modelling system (RAMS- DieCAST) to study a severe bora episode over the northern Adriatic Sea that occurred in January 1995. Both models were integrated at spatial resolution of 7 km. The 6-hour ECWMF analyses of wind, relative humidity, and temperature were used to provide the initial and lateral boundary conditions for the atmospheric model. A climatologically initialized, 3-month-long, stand-alone run of the ocean model provided initial conditions for the coupled system. Their results stress the importance of two-way coupling, even for small basins like the northern Adriatic, for quantitatively correct simulation of thermal changes. However, the ECMWF wind field was too coarse to depict the intricacies of the northern Adriatic gyral response. They obtained a very large cyclonic gyre that covered the greater northern Adriatic. The applied wind clearly missed the proper spatial structure. As a recent study of the Senj bora has shown [*Spoler-Canić and Kraljević*, 2005] even when the basic wind pattern is captured correctly, still finer model resolution (of the order of 1 km) is likely to be required to resolve the important details.

[8] *Wang* [2005] used a variant of POM to investigate a northern Adriatic bora event in January 2001. ECMWF wind stress and heat flux fields were again used. Numerous (30) Adriatic freshwater sources were represented as point or line source functions. The model was run for 25 months (1 January 1999 to 31 January 2001) on a regularly spaced, 5-km grid with 21 vertical sigma levels. With such a setup, it was possible to simulate the weak, baroclinic, pre-bora circulation and changes triggered by the mid-January bora. Like *Loglisci et al.* [2004], the study primarily demonstrated the bora impact on the northern Adriatic heat content (average heat loss of about 200 W/m^2). In contrast to other previous studies, but in accord with *Loglisci et al.* [2004], Wang also predicted a large cyclonic gyre over the extended northern Adriatic, missing the small-scale wind curl effect responsible for the double-gyre response. As pointed out in a recent paper [*Signell et al.*, 2005] the Adriatic wind fields derived from ECMWF forecasts are not only smoothed, failing to properly reproduce the spatial structure of the bora winds, but they also significantly underestimate the wind speed.

[9] The remainder of the paper is laid out as follows. The meteorological and oceanographic setup is presented in Section 2 and the field data in Section 3. The mathematical models used in the study are introduced in Section 4 and the numerical simulations elaborated in Section 5. The results are discussed in Section 6 and the conclusions presented in Section 7.

2. Meteorological and Oceanographic Setup

[10] The Adriatic bora is a downslope wind occurring on the lee side of the Dinaric Alps. Its onset, longevity, and severity are closely related to larger mesoscale flows [*Ivančan-Picek and Tutiš*, 1996] but ultimately controlled by local orographic features. Bora storms are connected to two typical weather patterns [*Yoshino*, 1976]. The cyclonic pattern (cyclonic bora, ''bora scura'') is characterized by a depression over the south Adriatic, pulling the colder continental air over the mountain passes. The pattern is accompanied by cloudy skies and occasional rain. The anticyclonic pattern (anticyclonic bora, ''bora chiara'') is marked by a high pressure system over Central Europe, without necessarily a well-developed cyclone over the Adriatic, pushing the colder continental air over the mountain passes. The pattern is accompanied by clear skies, and dry air. In either case, accumulation of cold air landward of the Dinaric Alps is essential as well as development a strong pressure gradient, across the mountain gaps in particular. The gaps exert orographic control over the air flow, producing lateral vorticity and ''fingers'' of higher wind speed (stress) leeward and offshore of the mountain range. Upstream accumulation of cold air is more likely to take place during the colder part of the year, so bora events occur more often during the winter.

[11] Northern Adriatic oceanographic conditions are strongly influenced by its physiographic features: the shallowness of the water column, the moderate bathymetric gradient, and the sizable riverine inflow [*Franco and Michelato*, 1992]. Progressive heat loss during the winter combined with wind-induced mechanical mixing destabilizes the water column and enforces almost complete vertical homogeneity. Lateral temperature and salinity variations persist throughout the winter period, primarily along the western coast, maintained by the freshwater inflow from the Po and other rivers. This view is reinforced by a recent review [*Poulain et al.*, 2001], and recently compiled temperature and salinity climatology (I. Janeković, internal report, 2005).

3. Data Collection and Reduction

[12] The January–February 2003 period considered in this study is characterized by several strong bora events.

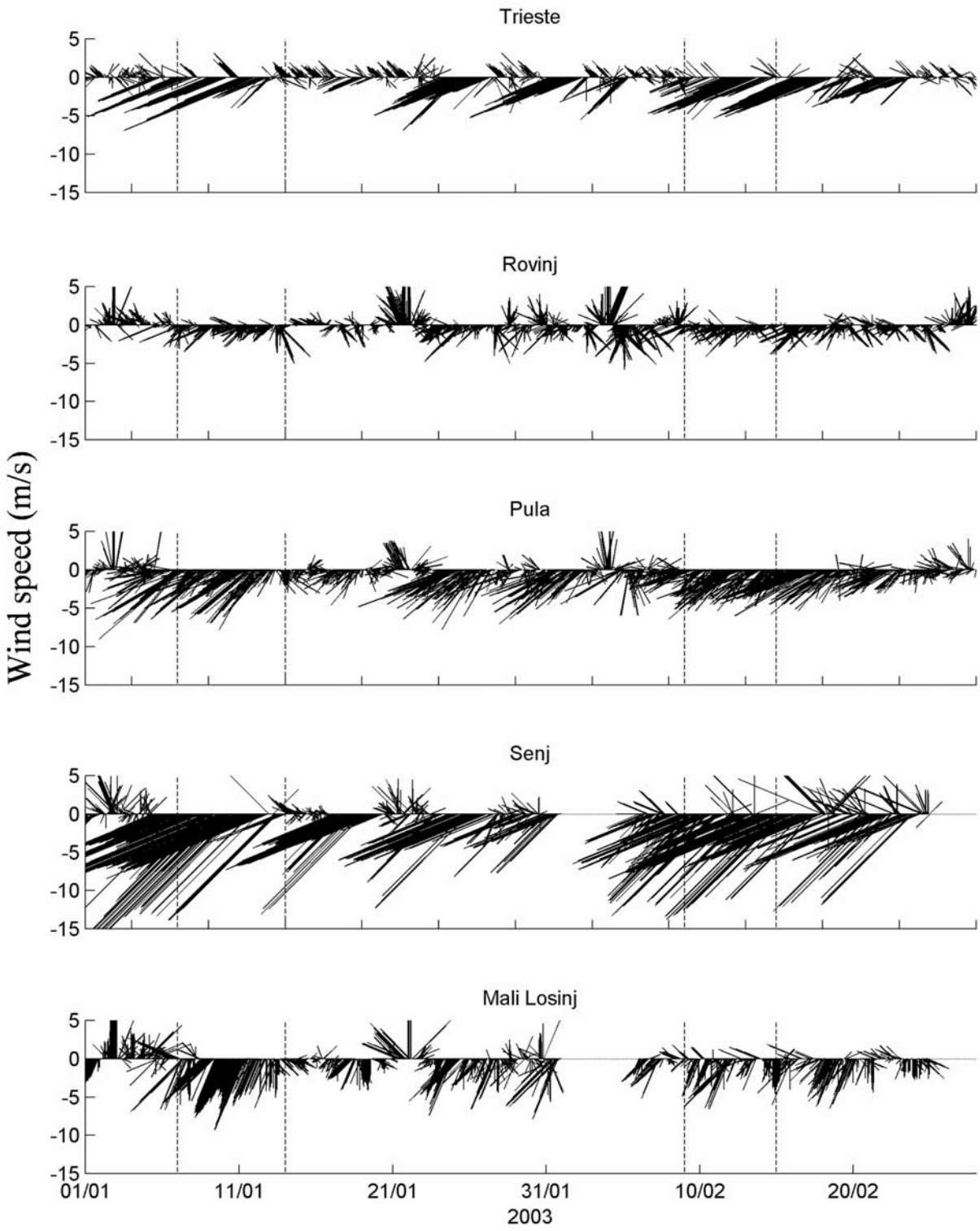

Figure 2. Stick plot of the 10-m, hourly wind registered at five east-coast stations during the January–February 2003 period. The dashed bars mark the beginning and end of the two prolonged bora episodes selected for study.

The January events were distinguished by pronounced cyclogenesis over the Tyrrhenian Sea and intense anticyclones over northwestern Europe imparting strong pressure gradients over the Dinaric Alps (B. Ivančan-Picek, personal communication). The mid-February bora event was provoked by a strong anticyclone north and northeast of the Alps. The January events fit the cyclonic bora classification by notable lack of AVHRR scenes (cloudiness). During the

mentioned period the 10-m wind was registered at several meteorological stations.

[13] A stick plot of hourly wind vectors (oceanographic convention) registered during the analysis period at 5 eastern Adriatic meteorological stations (Trieste, Rovinj, Pula, Senj, Mali Lošinj - Figure 1) is shown in Figure 2. The position of the Senj station has been suspected to cause under-representation of strong bora wind magnitude, while correctly registering the wind direction. In response to that concern, we have applied to the Senj magnitude recently derived correction factors, based on a comparison of wind magnitude at the regular and an auxiliary (better positioned) Senj station (Z. Bencetić Klaić, personal communication). The correction increased the wind magnitudes by 0.7, 2.7, 5.0, and 6.8 ms^{-1} in the 0–5, 6–10, 11–15, and >15 ms^{-1} magnitude ranges, respectively.

[14] One readily observes the prominence of northeasterly winds and their intermittent nature. Closer inspection of the figure reveals that the strongest wind was registered at the Senj station, whereas the Rovinj station, situated between the Trieste and Senj bora corridors, registered bora events of much lower intensity. One also notes the simultaneity of the Trieste and Senj bora events, but readily observes that they are not strictly coincident or of the same intensity or duration. If one selects the Senj record, takes the ENE and NE as bora directions, and sets 5 ms^{-1} as a threshold speed, two periods of unusually long bora duration emerge: 5–13 January and 9–17 February. If the speed threshold is lifted to 10 ms^{-1}, a somewhat shorter January period arises (7–13), while a gap of lower intensity bora appears in the other episode on 15 February, followed by two more bora events. The bora events in the Trieste time series appear more intermittent and of shorter duration compared to the Senj data. In addition to the stated magnitude and direction, we have required the parameters to apply for at least 3 days and be as applicable as possible to the Trieste record as well. With these requirements, we ended up with two representative bora events, one for January (7–13) and another for February (9–14) for closer modeling study and analysis. Both the Senj and Trieste series show several additional intense bora events of shorter duration and of lower Senj-Trieste simultaneity. It is understood that alternative bora event definitions are possible, but the one taken appears to serve well the stated purpose of the present study. For example, in their paper on marine atmospheric conditions and bora over the northern Adriatic, *Dorman et al.* [2006] declare existence of bora at their reference station when the wind is blowing from 60° (true north) with a speed greater than 2.6 ms^{-1} longer than 24 hours.

[15] Intensive international, multidisciplinary field studies undertaken in the northern Adriatic during winter 2002/03 documented its oceanographic conditions with an unprecedented level of observational intensity [*Lee et al.*, 2005a]. NRL and NURC jointly deployed 14 upward looking, bottom-mounted, Acoustic Doppler Current Profilers (ADCPs) [*Perkins et al.*, 2000] distributed along 3 transects in the northern Adriatic and one across Kvarner Bay. An additional upward-looking ADCP was mounted near the base of research tower Aqua Alta (VR1 in Figure 1). The circle-marked stations in Figure 1 have been used in present study. At the locations of the JRP moorings measurements were made of currents throughout the water column (by ADCP), bottom temperature (by ADCP and at some sites by wave/tide gauge), and bottom pressure (by ADCP or wave/tide gauge). To improve near-surface results by reducing surface wave aliasing, the JRP ADCPs were set to measure the currents using bursts of pings every 15 minutes at 1-Hz sampling frequency. Further processing details are given by J. W. Book et al. (Measurements of storm and nonstorm circulation in the northern Adriatic: October 2002 to April 2003, submitted to *Journal of Geophysical Research*, 2006, hereinafter referred to as Book et al., submitted manuscript, 2006).

Table 1. JRP and WISE ADCP Deployment Details[a]

Station	Longitude	Latitude	Depth	Cell	Observation Period
VR1	12.51	45.31	15.2	0.5	04.09.2002.–04.06.2003.
VR2	12.64	45.28	21.4	1	08.10.2002.–04.05.2003.
VR4	13.02	45.18	30.6	0.5	24.09.2002.–29.04.2003.
VR5	13.28	45.12	31.2	1	24.09.2002.–04.05.2003.
VR6	13.54	45.06	29.6	1	24.09.2002.–04.05.2003.
IC	13.59	44.85	41.2	2	20.12.2002.–07.03.2003.
CP5	13.62	44.68	43.9	2	20.12.2002.–07.03.2003.
CP2	12.86	44.46	38.4	1	23.09.2002.–28.04.2003.
CP3	13.13	44.54	38.4	1	23.09.2002.–04.05.2003.

[a]Stations coordinates are in degrees; location and cell depths are in meters.

[16] We have to point out here an anomalous result obtained for the VR5 station. Extensive ensuing analyses have demonstrated considerable directional discrepancy at VR5, at odds with results for the neighboring stations VR4 and VR6. Although no indication of instrumentation error was found, two separate tidal studies, one using an incremental-assimilation-augmented, very-high resolution Adriatic tidal model [*Janeković et al.*, 2004], and the other a strongly constrained assimilation of JRP current and pressure data (Book et al., submitted manuscript, 2006) have suggested the need for a directional clockwise correction of the VR5 tidal ellipses of 25° and 28°, respectively. Such a correction is also in accord with the bora field and modeling results of the present study. We have therefore decided to apply a directional correction to the VR5 data, opting for more conservative 25° value.

[17] The RBI WISE was conceived with a view to improve understanding of the northeastern Adriatic response to intense bora episodes and was partly modified at the final stage to fit the JRP mooring layout. The field component comprised deployment of three ADCPs in trawl-resistant bottom mounts (two are used in the present study: IC and CP5 in Figure 1). The WISE ADCPs used uniform 12-sec time gaps between pings, 2-m cells, and 10-min sampling periods. A raw data processing similar to the JRP procedure was applied to the WISE data, including the same response-method-based tidal signal removal and 2-hour low-pass data smoother. However, the surface echo interference was handled in a more restrictive fashion by excluding the contaminated surface bins for the whole measurement period. Mooring details for both field experiments are summarized in Table 1. Both the JRP and WISE data were further low-pass-filtered with an 8th-order Butterworth filter with a cutoff period of 24 hours (tides were already removed by the response method) to remove remaining shorter-period variance that we have not aspired

Table 2a. Low-Pass-Filtered Current Statistics: VR1[a]

Period	Depth	W	W_{max}	σ_T	θ	u	$\sqrt{\sigma_M}$	v	$\sqrt{\sigma_m}$	ε	γ
Jan-	1.7	14.1	36.7	79.1	54.8	12.9	9.7	1.6	3.8	0.39	
Feb	6.2	10.4	31.9	59.4	50.1	9.3	8.5	1.0	2.6	0.30	
	15.2	7.5	29.1	46.8	47.6	5.8	8.1	−02	2.1	0.26	
	vbar	9.4	30.6	56.7	48.7	8.6	8.2	0.4	2.0	0.25	0.87
Jan	1.7	16.3	31.7	82.8	55.8	15.8	9.0	2.3	1.8	0.19	
episode	6.2	15.7	31.9	78.7	55.4	15.1	9.4	2.6	1.6	0.17	
	15.2	13,2	27.0	62.8	46.5	13.0	8.1	0.1	1.7	0.21	
	vbar	15.1	30.3	75.8	54.1	14.7	9.0	2.0	1.5	0.17	0.98
Feb	1.7	20.0	30.5	35.7	52.3	19.8	6.0	2.6	1.2	0.20	
episode	6.2	18.6	30.3	39.6	59.8	17.8	6.5	4.6	1.4	0.21	
	15.2	14.4	26.7	50.6	48.8	14.1	7.4	−0.4	1.9	0.25	
	vbar	17.5	29.5	43.1	57.6	17.1	6.7	3.5	1.2	0.18	0.93

[a]W, mean speed; W_{max}, maximum speed; σ_T, total variance; θ, direction of the major axis; u, mean current along major axis; $\sqrt{\sigma_M}$, standard deviation along major axis; v, mean current along minor axis; $\sqrt{\sigma_m}$, standard deviation along minor axis; $\varepsilon = (\sigma_m/\sigma_M)^{1/2}$, polarization of the flow; γ, current depth dependence; vbar marks the column averaged values. Depth is in meters, speed is in cms^{-1}, angle in degrees north.

to reproduce with the models. Current statistics for a three-station subset of the nine JRP/WISE stations used in the present study are summarized in Tables 2a–2c for the whole January–February period as well as for the selected bora events. The calculated statistics includes the mean and maximum speed (W and W_{max}), total variance (σ_T), orientation of the principal axis of variability, mean currents and their standard deviations along major and minor principal axes (θ, u, $\sqrt{\sigma_M}$, v, and $\sqrt{\sigma_m}$, respectively), polarization (ε), and current-depth dependence (γ) calculated following the work of *Thompson and Pugh* [1986] as:

$$\gamma = \frac{N(\overline{\sigma}_M - \overline{\sigma}_m)}{\Sigma(\sigma_M^i + \sigma_m^i)} \quad (1)$$

where N is the number of depth cells used to form the depth mean, i is the index of the depth cell summation, and the overbar indicates the principal variances of the depth-mean current. Principal component analysis [*Emery and Thompson*, 1997] was used to calculated the values of σ_M, σ_m, and Θ. The selected stations (VR1, IC, and CP5) demonstrate the dominant response. At VR1 (more influenced by the Trieste bora), one can readily observe that the time- and depth-averaged speed is twice as large during the bora episodes than for the whole period. For both episodes, the axis of principal variance follows the local coastline to within 3–4°, but some other parameters exhibit inter-episodic differences. Compared to February, the January ε and γ values suggest more polarized and more depth-independent motion, but smaller averaged velocity along the axis of principal variance. The case is opposite at CP5, a station more sensitive to the Senj bora, where the January episode is characterized by less rectilinear and more depth-dependent flow. There is also a factor of 2.5 difference in the inter-episodic orientation of the principal axis. The IC station is in the wind-quiet region between the Trieste and Senj bora corridors with clearly lower average speeds and less polarized flow. The CP2 data for both episodes (not tabulated) exhibit even lower average and maximum speed values. Tabulated surface, middepth, and bottom values suggest that during the winter of 2003 and the bora episodes in particular, the northern Adriatic water column can be viewed as a single layer. We will return to these statistics in later sections when analyzing the modeling results.

[18] A scatterplot of the vertically averaged currents for all nine stations and the two bora episodes, given in Figure 3, provide additional insight. For both episodes, five self-similar groups can be identified in the figure. The VR1 and VR2 plots show downwind transports whereas stations VR4 and VR5 show a return, upwind flow. The third group (VR6 and IC) suggests anticyclonic motion along the west Istrian coast. The CP stations 3 and 5 indicate the existence of another cyclonic cell, while CP2 appears outside any of the mentioned circulation structures.

4. Numerical Models

[19] Three numerical models were used in this study, one atmospheric, and two oceanic. The atmospheric portion of

Table 2b. Low-Pass-Filtered Current Statistics: IC[a]

Period	Depth	W	W_{max}	σ_T	θ	u	$\sqrt{\sigma_M}$	v	$\sqrt{\sigma_m}$	ε	γ
Jan-	7.2	5.3	16.7	11.5	−65.6	−2.2	5.4	−0.2	2.5	0.46	
Feb	19.2	4.8	15.6	10.9	−63.8	−2.4	4.9	0.4	2.1	0.43	
	39.2	4.4	13.1	7.7	−52.6	−3.0	3.8	0.4	2.0	0.54	
	vbar	4.6	14.8	9.8	−61.6	−2.5	4.5	0.4	2.0	0.43	0.93
Jan	7.2	9.6	16.7	19.5	−80.8	−8.8	4.9	2.6	2.1	0.43	
episode	19.2	9.3	15.6	17.4	−85.2	−7.7	4.9	3.6	2.5	0.51	
	39.2	7.9	13.1	10.0	84.6	−5.6	3.8	4.3	2.6	0.68	
	vbar	8.9	14.9	14.9	−87.9	−7.2	4.5	3.8	2.4	0.54	0.97
Feb	7.2	4.9	8.2	4.1	−88.7	−2.8	4.1	−1.0	1.8	0.43	
episode	19.2	4.5	7.4	3.4	−80.8	−2.4	3.9	−0.1	1.7	0.44	
	39.2	4.1	7.1	4.5	−75.0	−3.0	3.1	0.6	1.7	0.54	
	vbar	4.3	7.3	3.8	−79.6	−2.6	3.6	0.1	1.5	0.42	0.94

[a]As in Table 2a.

Table 2c. Low-Pass-Filtered Current Statistics: CP5[a]

Period	Depth	W	W_{max}	σ_T	θ	u	$\sqrt{\sigma_M}$	v	$\sqrt{\sigma_m}$	ε	γ
Jan-	7.9	10.1	38.5	62.0	11.8	8.5	8.8	−0.6	3.8	0.43	
Feb	21.9	9.1	36.6	56.2	11.2	7.7	8.2	−0.4	3.5	0.43	
	39.9	8.2	33.0	45.0	14.5	6.7	7.4	−1.4	3.5	0.47	
	vbar	8.8	35.2	53.2	12.1	7.4	7.9	−0.8	3.4	0.42	0.96
Jan	7.9	19.4	38.1	99.0	6.1	17.6	11.5	−2.9	4.9	0.43	
episode	21.9	17.8	36.3	97.6	6.6	16.4	10.8	−2.3	4.9	0.45	
	39.9	15.4	33.1	86.3	11.6	14.3	9.8	−2.0	4.3	0.44	
	vbar	17.2	35.3	94.5	7.6	15.9	10.5	−2.4	4.5	0.42	0.96
Feb	7.9	12.4	23.5	38.0	19.0	12.1	6.3	1.5	1.9	0.30	
episode	21.9	11.6	22.8	36.0	19.1	11.3	6.2	1.9	1.4	0.23	
	39.9	10.6	20.5	30.7	29.8	10.2	5.7	2.3	1.4	0.25	
	vbar	11.3	21.7	34.5	21.8	11.0	6.0	1.9	1.2	0.19	0.96

[a]As in Table 2a.

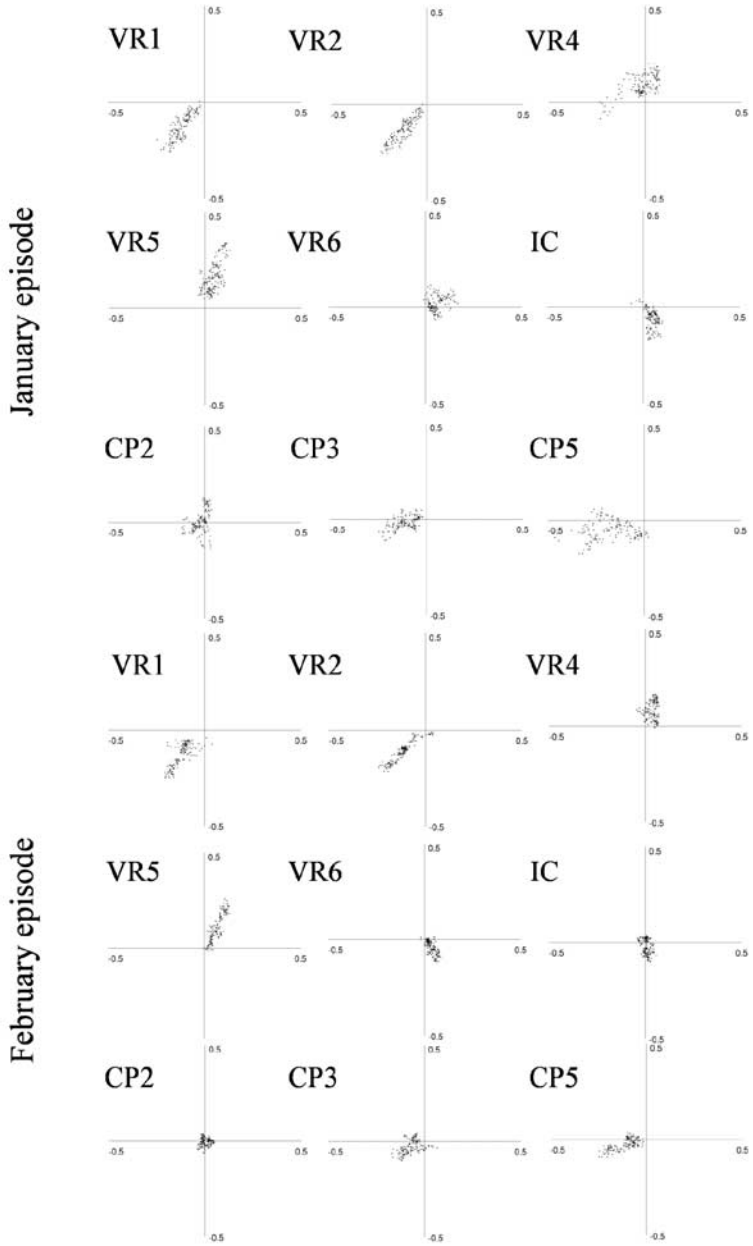

Figure 3. Scatterplot of the low-pass-filtered, vertically averaged currents measured at nine stations during the January and February bora episodes.

the COAMPS [*Hodur*, 1997] was applied in a reanalysis mode in order to generate atmospheric forcing fields needed to drive the oceanic models. The COAMPS atmospheric model is a finite-difference approximation to the fully compressible, non-hydrostatic equations. Physical parameterizations are used to represent surface fluxes, boundary layer mixing, radiation, and moist processes including microphysical quantities [*Hodur*, 1997]. The initial fields for the model are created from multivariate optimum interpolation analyses of upper-air soundings and surface, commercial aircraft, and satellite data that are quality controlled and blended with the 12-h COAMPS forecast fields. The data assimilation is accomplished through an incremental update procedure that enables mesoscale phenomena to be retained in the analysis increment fields. The lateral boundary conditions for the outermost mesh make use of Navy Operational Global Analysis and Prediction System (NOGAPS) forecast fields. The domain configuration for these reanalysis simulations contains three horizontally nested grid meshes with horizontal grid resolution of 36, 12, and 4 km, respectively. The 4-km resolution grid mesh is centered over the Adriatic Sea. The model is configured with 30 vertical levels on a non-uniform vertical grid consisting of an increment of 10 m at the lowest level. The topographic data for the atmospheric simulations are based on the National Imagery and Mapping Agency (NIMA) 1-km resolution data set that enables the prominent orographic features, and the Dinaric Alps in particular, to be resolved. Additional details of the COAMPS reanalysis can be found in *Pullen et al.* [2003].

[20] The first ocean model used here is NCOM as described by *Martin* [2000], with some improvements as reported by *Morey et al.* [2003] and *Barron et al.* [2005]. This model is similar in its physics and numerics to POM [*Blumberg and Mellor*, 1987], but uses an implicit treatment of the free surface and a hybrid vertical grid with sigma coordinates in the upper layers and (optionally) level coordinates below a user-specified depth. For the results presented here, a third-order upwind scheme [*Holland et al.*, 1998] was used for advection, vertical mixing was computed using the Mellor-Yamada Level 2 scheme [*Mellor and Yamada*, 1974], which is modified for use over the entire water column, and density was computed using the equation of state of *Mellor* [1991]. The model domain consists of the entire Adriatic Sea including the Strait of Otranto. The horizontal grid resolution is 1 km. The vertical coordinate consists of 32 layers, with 22 sigma layers between the surface and a depth of 290 m and level coordinates below 290 m. Hence, the grid is like a regular sigma coordinate grid in water shallower than 290 m and is similar to a level grid where the bottom depth is greater than 290 m. The static thickness of the upper layer is 2 m where the bottom depth exceeds 290 m and is reduced in shallower water where the sigma-coordinate grid is compressed. The time step was 200 s.

[21] The second oceanic model is a variant of the finite element model QUODDY with some improvements based on the 3D, non-linear, shallow-water equations [*Lynch et al.*, 1996]. The Level 2.5 turbulence-closure scheme of *Mellor and Yamada* [1982] is used with improvements described by *Galperin et al.* [1988]. The horizontal diffusion parameterization scheme is that of *Smagorinsky* [1963]. A free-slip condition is imposed along the coast. The details of the model solution on a finite element grid are described by *Lynch and Werner* [1991]. Bottom stress is estimated from the classical quadratic law as a function of bottom velocity. The well-known sigma-coordinate system is used in the vertical with 21 non-uniformly placed nodes whose sinusoidal vertical spacing provides increased resolution in the surface and bottom layers. The unstructured model mesh consists of 28669 elements and 17284 nodes with minimal nodal distances found in the coastal areas of about 100 m and minimal element size about 9000 m^2. Maximal nodal distances of 5500 m are found in the middle of the domain. With the southern open boundary set at 43.5°N, the model domain covers part of the central and the entire northern Adriatic. In accord with the CFL criterion, the model time step was set to 5 s. Atmospheric forcing was provided by hourly COAMPS re-analysis 10-m wind fields.

5. Computer Simulations

[22] A sequence of numerical experiments was conducted in order to re-examine the question of the double-gyre response. Simplified, feature-oriented numerical simulations were carried out using the QUODDY model whereas the reference bora event simulations were taken from the long, "everything included" NCOM Adriatic run. In accord with previous experience, the episodic, bora-event QUODDY simulations were initialized from rest with a spinup time of several days. A value of 0.003 was used for the bottom drag coefficient, based on previously performed numerical experiments and reported literature values. At the surface the drag coefficient was defined according to *Large and Pond* [1981]. The river inflows were not simulated. Tidal forcing was not included in the QUODDY simulations, although a separate tidal study was made [*Janeković and Kuzmić*, 2005].

[23] The NCOM Adriatic simulation was initialized on 1 September 2002 with fields from a hindcast of NRL's global NCOM model [*Kara et al.*, 2005]. Boundary conditions at the open boundary in the northern Ionian Sea were provided by daily values of surface elevation, velocity, temperature, and salinity from the global model. Tidal forcing was provided at the open boundaries using tidal data from the Oregon State University (OSU) tidal databases, which are derived from satellite altimetry data [*Egbert and Erofeeva*, 2002]. Data from the OSU regional Mediterranean database were used for the K1, O1, M2, and S2 constituents and data from the OSU global database were used for P1, Q1, K2, and N2. Tidal potential forcing for these eight constituents was used in the interior of the model domain. Atmospheric forcing was provided by hourly COAMPS re-analysis fields of surface air pressure, wind stress, solar radiation, net longwave radiation, and precipitation [*Hodur*, 1997]. Latent and sensible heat fluxes were computed using standard bulk formulas, the COAMPS 10-m wind speed and 2-m air temperature and humidity, and the NCOM model SST. The stability-dependent *Kondo* [1975] drag coefficient was used for the bulk flux calculations with neutral values of 0.0014 and 0.0011 for the latent and sensible fluxes, respectively. River and runoff inflows for the Adriatic were taken from the monthly climatological database of *Raicich* [1994]. The discharges for 39 Adriatic rivers were specified

at the closest coastal model grid point to the river-mouth location and runoff inflows were distributed along the appropriate sections of coastline. Daily observed discharge values were used only for the Po River (obtained from Alessandro Allodi at the Ufficio Idrografico del Magistrato per il Po, Parma, Italy). The model was run to the end of March 2003 and model fields were saved every 3 h for analysis and comparison with observations.

[24] Numerical experiments were conducted to address three related response issues: the time-variable bora wind, the gyral-response pattern, and the extrusion of colder/freshened waters. The KO paper dealt with these issues under simplified and therefore restrictive assumptions. The key issue of this revisit is thus the wind-imparted, double-gyre pattern with additional aspects that accompany bora events: the cross-basin protrusion of freshened water and pronounced heat loss at the air-sea interface. The issues are directly related to the state of the atmosphere above the northern Adriatic and its effect imparted on the NCOM and QUODDY model solutions via the COAMPS-derived forcing.

[25] To address the first issue, the COAMPS 10-m wind field time series for the two selected bora episodes were compared to wind measurements at five coastal stations (Trieste, Rovinj, Pula, Mali Lošinj, and Senj). Both models were used to address the second issue, to try to confirm the mechanical, essentially barotropic nature of the double-gyre response. To that end, the selected bora events were studied using barotropic, wind-only, single-episode, QUODDY runs and appropriate segments of the baroclinic, all-fluxes-included, long-series, NCOM run. The output of both models was validated by comparison to the JRP/WISE ADCP current meter data. While dealing with the third issue, the offshore protrusion of freshened (riverine) and cooled coastal waters were used to trace the spinup of the northern (Trieste) cyclonic gyre. This part of the study was aided with locally received AVHRR data processed to obtain analyzed SST fields. The impact of cooling heat exchange at the air-sea interface was also addressed in this experiment. To that end, the NCOM 16–27 February 2003 simulated sequence of 3-hourly solutions provided the reference case. The QUODDY model, started from homogeneous winter conditions (8°C, 38 psu) and forced with COAMPS 10-m winds plus NCOM-corrected COAMPS surface heat fluxes, provided the auxiliary run useful in elucidating the impact of the heat-flux inclusion.

6. Results and Discussion

6.1. Variable Wind Forcing and Gyral Response Pattern

[26] In the KO paper, the double-gyre response was studied using a coarser grid and bathymetry (7.5-km resolution), a smaller basin (down to the Pula-Pesaro line, Figure 1), and a climatological, steady wind forcing. In the present study, a more than twice-larger modeled area was covered with QUODDY, and the whole Adriatic with NCOM. An order-of-magnitude finer grid was used (with commensurate bathymetry) as well as forcing with wind akin to its true variability in space and time. The quality of the COAMPS atmospheric reanalysis surface fields, which were used to force the sea models, is illustrated by comparison of the simulated winds with observations at three meteorological stations (Figure 4). Several bora-intensity oscillations occurred during selected January and February episodes.

[27] At the Pula station, the COAMPS simulation captures promptly and accurately the events of the strengthening northeasterly winds and the relatively quiescent periods between events. The model simulations overall capture the duration of the strong-wind-speed event and generally reproduce well the magnitude of the events. However, the model slightly under-forecasts the magnitude of several of the bora peaks, such as on 7 and 9 January, and over-forecasts the speed maximum on 12 January and 12 February. The differences between the model-simulated and observed maxima typically fall in the range of $2-5\ \mathrm{ms}^{-1}$.

[28] The COAMPS winds compare reasonably well with the observations at Trieste as well, but the model, in general, tends to overpredict the wind magnitude. The model-to-data discrepancies observed at several current stations, presented later in this section, support this conclusion. However, *Signell et al.* [2005] found that, compared to wind observed at the oceanographic tower Aqua Alta (our station VR1), COAMPS predicted well a March 2001 bora, slightly under-estimating its magnitude.

[29] Notable differences between the simulated and observed winds are also observed at the Senj station. For example, the model predicts rather successfully the onset, duration, and magnitude of the 9–10 January bora event, but then significantly over estimates the strength of the next peak. A similar effect is observed in the February episode. Some of these discrepancies possibly arise from small-scale features in the coastal topography, which are likely important for the local-scale structure of the bora, but which may be smoothed or not completely resolved in the 4-km horizontal resolution COAMPS. In line with that reasoning one notes that COAMPS excels at Pula, which is surrounded by low and fairly smooth orographic features, but shows larger differences at Trieste and Senj, where orographic gradients are more pronounced. Additionally, wind speed time series constructed for the four COAMPS grid points surrounding Senj (not shown) indicate substantial sensitivity.

[30] Vorticity in the wind field imparts a generic pattern on the northern Adriatic circulation. Several requirements have to be met before this sea response is properly simulated. The first and foremost is the spatial resolution of the forcing wind field. A previous study [*Kuzmić et al.*, 1988] provides evidence that it should not be much coarser than about 15 km. Provided that the resolution requirement is fulfilled, the skill in predicting the onset and spatial extent of the gyres and the proper magnitude and direction of the bora-induced currents determines the eventual success of a particular model and/or simulation.

[31] It has been shown in the KO paper that the frictional adjustment times of the shallow, northern Adriatic are much shorter than the typical duration of the atmospheric disturbances, assuring its prompt accommodation to the wind forcing. Furthermore, lateral variability in the bora wind field imparts a much richer response than mere convergence against the Italian coast would produce. A snapshot of transient response, obtained with the COAMPS-forced QUODDY model, is depicted in Figure 5 for both the

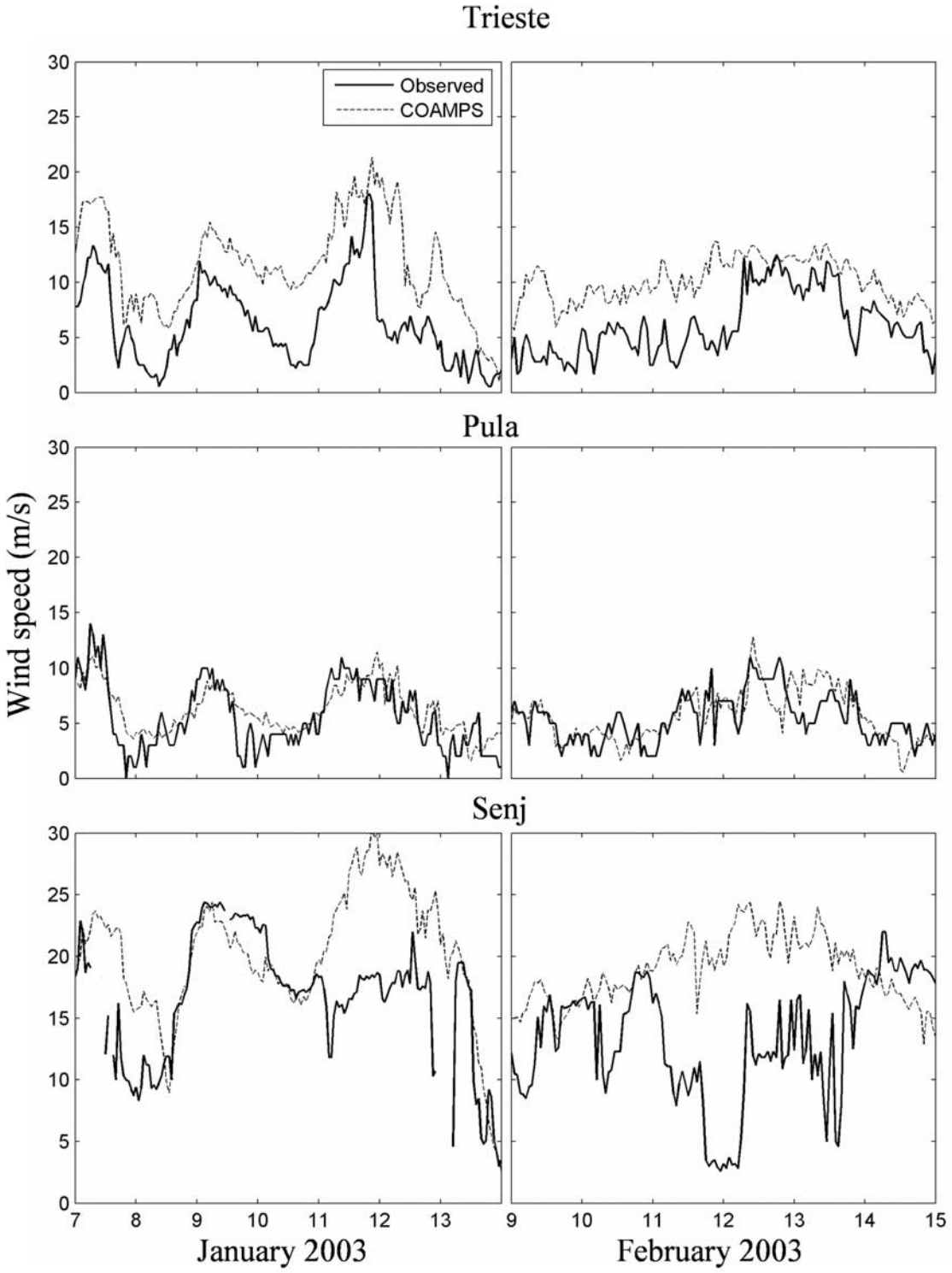

Figure 4. Observed (solid) and COAMPS-predicted (dashed) hourly wind speed at the Trieste (top), Pula (middle), and Senj (bottom) stations during the selected bora episodes in January (left) and February (right) 2003.

January (top) and February (bottom) episodes. Enhanced surface wind stress below the Trieste and Senj bora jets generated southwestward transports and convergence against the western coast. The convergence imparts a sea-level slope that drives a southward flow. However, the wind vorticity and the related subsidence of the wind between the two jets (see the Rovinj station data in Figure 2) modify the convergence. Consequently, the upper (Trieste), and lower (Senj) cyclonic gyres are formed around the corresponding lows of the sea-surface height. The basin east- and west-side

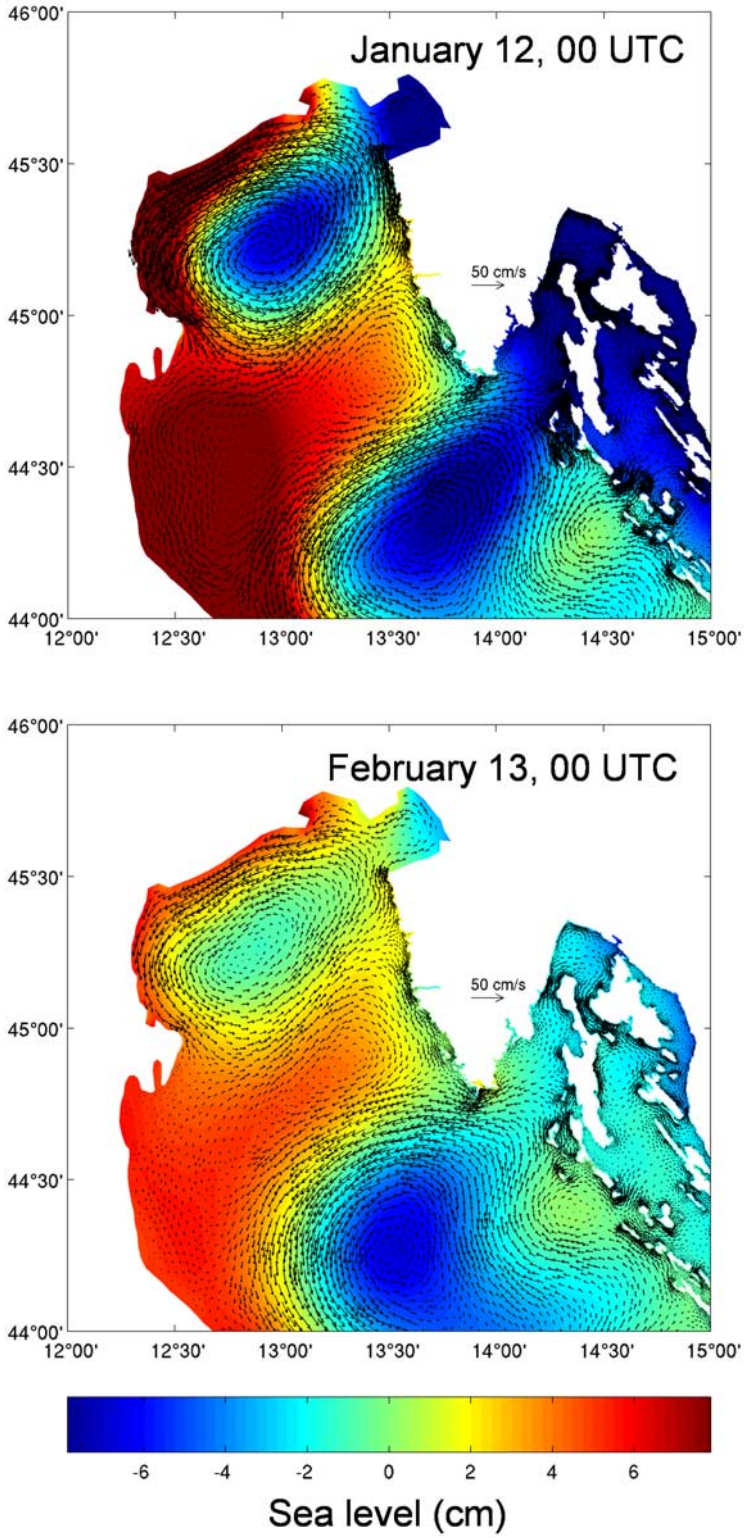

Figure 5. A snapshot of the sea level and circulation transient response to the January (top) and February (bottom) bora episode as simulated with the QUODDY model started from rest and forced with COAMPS winds.

waters in the area between the two cyclonic gyres respond differently to the establishment of the gyres. In the deeper, eastern part, which is bounded on its northern and southern sides by flows of opposite direction, an anticyclonic (Rovinj) gyre is formed. In the shallower western part, which is under stronger slope control, and more immediate Po River and Senj gyre influence more transient patterns develop. In this area two opposing, southward- and west-

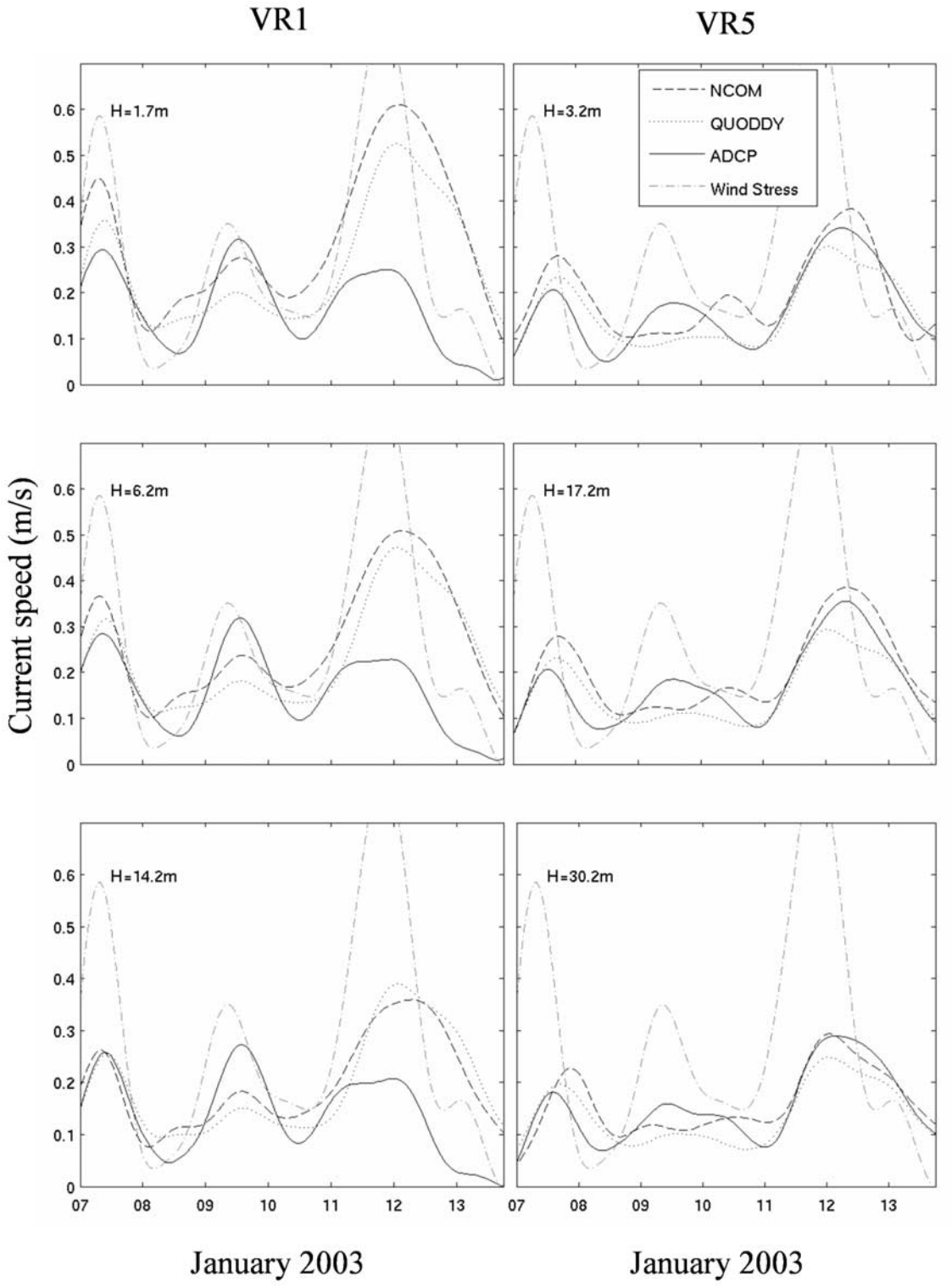

Figure 6. Measured (ADCP) and modeled (NCOM, QUODDY) low-pass-filtered current speed at stations VR1 (left), and VR5 (right) at the depth of the surface (top), middle, and bottom cell location during the January bora episode. Also plotted is the COAMPS wind stress at the Trieste station in N/m^2 scaled by 0.5 to fit the current speed axis. The x axis denotes days in January.

ward-directed flows have to accommodate each other (see Figure 12 and discussion later on), and their strength and directional changes control the interplay. The Trieste and Senj cyclonic gyres and the Rovinj anticyclonic gyre appear to be permanent features of the response, with details that may vary from one bora event to another. We will examine next from both observational and modeling side the details of the response at the ADCP station locations, starting with the Trieste gyre.

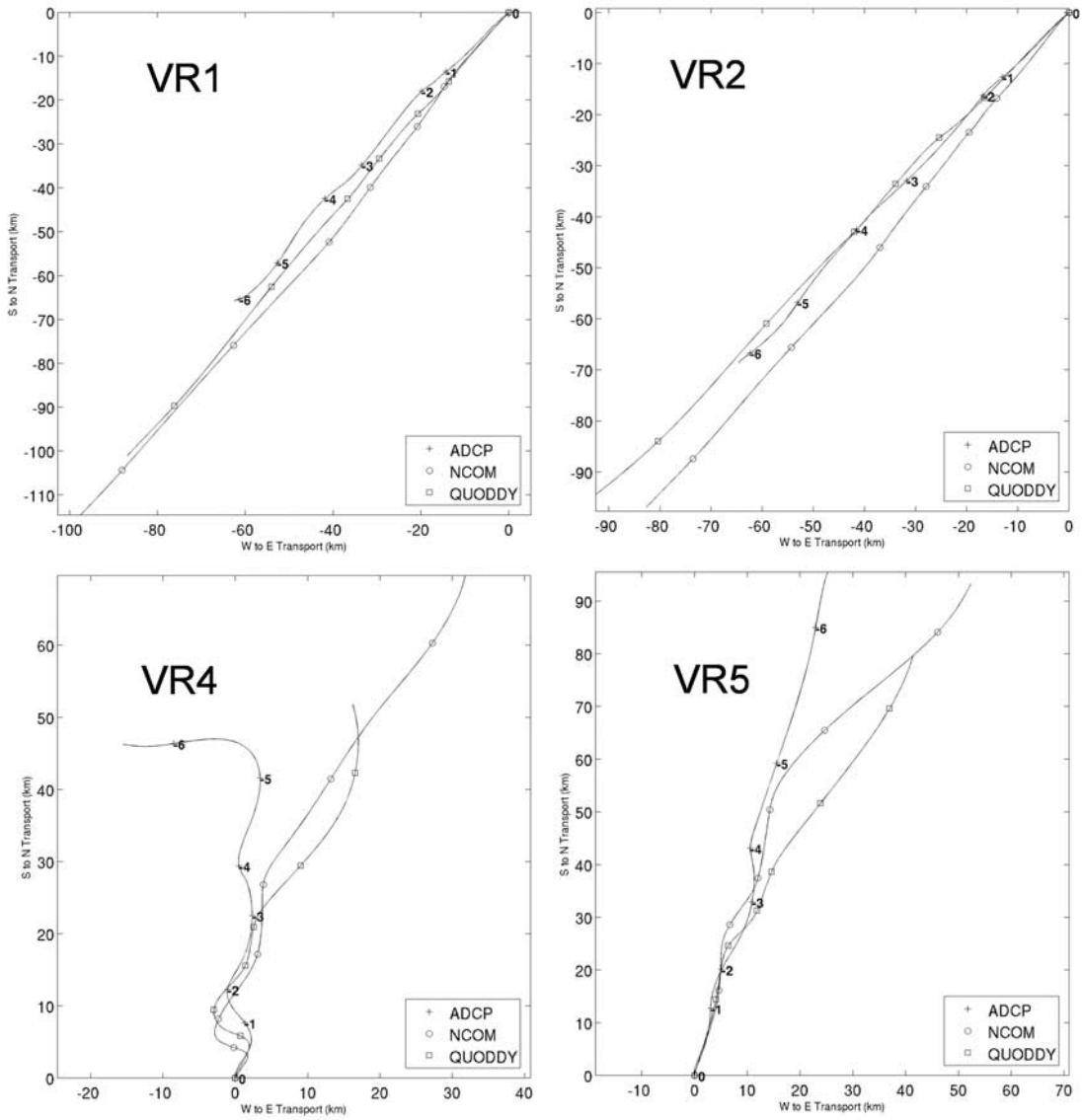

Figure 7. Progressive vector diagram of the vertically averaged, low-pass-filtered currents at stations VR1 (top left), VR2 (top right), VR4 (bottom left) and VR5 (bottom right) derived from the ADCP measurements (pluses), the NCOM model (open circles), and the QUODDY model (open squares) for the January bora episode. Numbers mark the number of days since 7 January.

[32] In a shallow, unstratified water column, wind-stress-imparted momentum is transferred downward expediently, so currents along the northwestern coastal strip respond quickly to an onset of bora wind. The simple analytical model of *Schwing et al.* [1985] for a shallow, coastal stretch of constant depth can be used to infer the phase relations between the wind and transports. In this frictionally dominated situation, with an offshore distance of 10 km, a depth of 15 m, and a wind period of 2 days, the model predicts establishment of alongshore transport at VR1 lagging the wind by 0.5 hrs. Low-pass-filtered-current magnitudes, observed and modeled at the surface (top), midcolumn (middle), and bottom depths of VR1 (left) and VR5 (right) are depicted in Figure 6. The wind and currents appear correlated, and several things are readily apparent. The current response is rather barotropic and the bora signal is transmitted down to the bottom. The models reproduce that with remarkable success regarding the timing and magnitude of the bora-induced peaks, relative to the observations. The two models forced with the same wind, but otherwise different in many design and forcing aspects, produce current magnitude predictions generally following each other. Both models underpredict the 9–10 January peak, and drastically overpredict the 11–13 January peak. One notes at VR5 better correspondence between the observed and modeled peak magnitudes and timing, for the period 11–13 January in particular. Progressive-vector-diagram (PVD) plots of the vertically averaged currents at VR1 and VR2 for the same episode (Figure 7, top) offer additional insight. The plots provide pseudo-Lagrangian information, which is more susceptible to directional differences. In accord with the shallowness and lateral con-

straints, the measured and modeled paths at VR1 and VR2 closely follow each other throughout the six-day period (the ADCP and QUODDY path at VR2 in particular). The longer modeled paths at both locations are a consequence of over-predicting the current speeds. The February episode (not shown) pictures essentially the same situation with 20–30 km shorter paths.

[33] The old KO simulations showed that in a flat-bottom northern Adriatic, Coriolis-deflected sea-surface slope is established within a day. When the basin is driven by a horizontally varying wind field, variations in both depth and wind stress become important. Bathymetric and wind effects can be evaluated using the linearized, conservation of mean flow vorticity equation [*Csanady*, 1975]:

$$\frac{\partial}{\partial t}\left(\frac{\partial \overline{v}}{\partial x}-\frac{\partial \overline{u}}{\partial y}\right)=curl\left(\frac{\tau}{h}\right) \tag{2}$$

where $\overline{u}$ and $\overline{v}$ are depth-averaged velocities, τ is the wind stress vector, and h is the water depth. If the relative change of the wind stress is greater than the topographic variation (which is the case in the northern Adriatic), the wind variations dominate. As pointed out a long time ago [*Shtokman*, 1941], in such situations, lateral heterogeneities in the wind field produce circulations that close both horizontally and vertically, resulting in an upwind surface flow at some locations. Such a situation is observed at stations VR4 and VR5. In contrast to VR1 and VR2, where the slope currents, developed in response to the cross-shore Coriolis force, reinforce the drift currents, at VR4 and VR5 the slope currents oppose a weaker, stress-imparted drift and the net flow is upwind (Figure 7, bottom). One readily notes that at both VR4 and VR5 model predictions closely follow the observations until 10 January, and disagree more in the second part of the January episode. Inspection of Figure 4 shows generally better COAMPS-magnitude-to-data agreement during the first part of the January episode.

[34] The area southeast of the Trieste gyre responds to the bora with a cell circulating in the opposite direction (see Figure 5). But here the intensity of the currents is much lower and the model/observations discrepancy is much higher than at the stations under direct bora forcing. At both the VR6 and IC stations and for both bora episodes (with the partial exception of VR6 in January), the current data clearly trace a part of the southeasterly directed (anticyclonic) flow (Figure 8). In terms of the vertically averaged, low-pass-filtered, progressive current vectors, the model-to-data agreement is highest at VR6 in February and lowest at IC in January. The agreement between the models (in spite of the same wind-field forcing) is much lower than at the other VR stations, with occasional, completely opposite direction of the predicted flow (at IC in January). Very similar PVD paths are obtained for the surface bin positions at both stations and for both episodes (not shown).

[35] Modeled and observed speed at CP3 and CP5 during the January episode is plotted in Figure 9. As in Figure 6, the surface response is plotted at the top, the midcolumn response in the middle, and the bottom-cell level response speed in the lowest row. The CP3 station exhibits currents of lower intensity than at VR1, but both models as before predict mutually similar speed values. The most problematic again is the end of January episode, with both models notably overpredicting the speed. The situation is worse at CP5 where both models first underpredict the speed and then grossly overpredict it by the end of the episode. Inspection of the Senj wind in Figure 4 points to the wind field as the cause of the discrepancy. The PVD paths in Figure 10 for CP3 (middle), and CP5 (bottom) show the models overpredicting the northward flow at CP5 and the southward flow at CP3. At the westernmost station, CP2, both models predict a steady southward movement at odds with the ADCP data, which exhibits much slower eastward flow.

[36] In order to gain additional insight and to compare more formally the differences between the measured and modeled response, several useful ratios are introduced [*Schwab et al.*, 1989]. Specifically:

$$r_x=\frac{\Sigma\left[(u_x-\overline{u}_x)^2+(v_x-\overline{v}_x)^2\right]}{\Sigma\left(u_x^2+v_x^2\right)} \tag{3}$$

where r_x is the ratio of the time-variant current energy to the total current energy with x equal to O(bserved), N(COM) or Q(UODDY)–summation is over hourly values within selected period;

$$r_{xy}=\frac{\sqrt{\Sigma\left(u_y^2+v_y^2\right)}}{\sqrt{\Sigma\left(u_x^2+v_x^2\right)}} \tag{4}$$

$$rt_{xy}=\frac{\Sigma\left[\left(u_x-u_y\right)^2+\left(v_x-v_y\right)^2\right]}{\Sigma\left(u_x^2+v_x^2\right)} \tag{5}$$

$$rv_{xy}=\frac{\Sigma\left[\left[(u_x-\overline{u}_x)-\left(u_y-\overline{u}_y\right)\right]^2+\left[(v_x-\overline{v}_x)-\left(v_y-\overline{v}_y\right)\right]^2\right]}{\Sigma\left[(u_x-\overline{u}_x)^2+(v_x-\overline{v}_x)^2\right]} \tag{6}$$

$$rm_{xy}=\frac{\left(\overline{u}_x-\overline{u}_y\right)^2+\left(\overline{v}_x-\overline{v}_y\right)^2}{\overline{u}_x^2+\overline{v}_x^2} \tag{7}$$

where r_{xy} is the ratio of the root mean square (RMS) of the computed currents to the RMS of the observed currents, rt_{xy} is the ratio of the computed and observed total flow, rv_{xy} is the ratio of the computed and observed time-variable flow, and rm_{xy} is the ratio of the computed and observed time-mean flow; the xy equals ON or OQ. The comparison is summarized in Tables 3a–3c. At VR1, both the observed and modeled r_x values are less than 0.2 for both episodes (with the exception of r_O for January), indicating high values of episode-averaged mean energy. At CP5, the upper limit for r_x is almost twice as high (0.388), suggesting a proportionally lower episode-averaged mean. The r_x values are highest at IC where episode and depth-averaged speeds exhibit the lowest values and time-variable energy can account for more than 80% of the total energy. Both models underpredict this ratio for both episodes at the directly wind-forced stations (VR1 and CP5), with the exception of QUODDY at CP5. At IC, the models exhibit rt and rv ratios greater than one, with NCOM providing a factor of 3–5

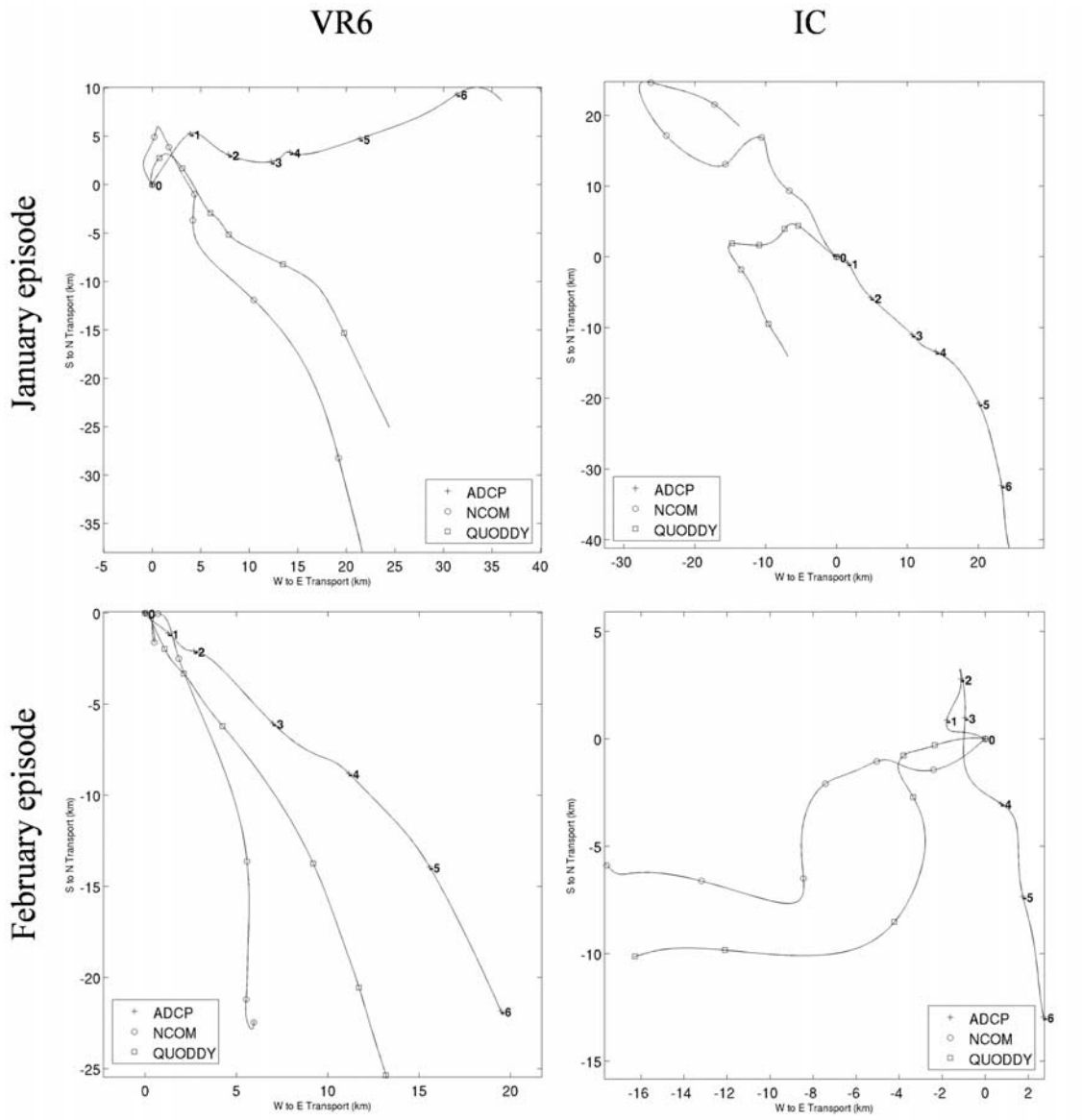

Figure 8. Progressive vector diagram of the vertically averaged, low-pass-filtered currents at stations VR6 (left) and IC (right) for the January (top) and February (bottom) episodes. Numbers mark the number of days since 7 January and 9 February, respectively.

larger variability than observed in the data. The RMS values of the computed currents are always higher than the respective observed values for NCOM (indicating over prediction) and lower than observed for QUODDY (with the exception of VR1 for January and IC for February).

[37] Calculated observed/model differences for the total, time-variable, and mean flow provide additional insight. At all stations, QUODDY gives smaller rt values than NCOM for both episodes, suggesting smaller depth- and episode-averaged discrepancies with the observed total flow. The same is true for both the time-variable and mean component of the flow, with the exception of the VR1 value for January. Even that exception appears to be related to anomalously low rv_{ON} values near bottom. The QUODDY-calculated mean currents agree rather well with the observed means at VR1 and CP5 and clearly not so well at IC. At all three stations and for both episodes, the QUODDY differences with the observed are variously smaller than NCOM. One possible explanation is that NCOM accumulated over the previous simulated months a component of the flow, for which the episode-focused QUODDY did not have the time. Discrepancies in the calculated, time-variable parts of the currents exceed the respective observed variability for both models and all stations and episodes; for NCOM the rv_{xy} ratio reaches a value of 5.70 at the IC surface in the January episode and drops down to 1.20 at the VR1 bottom in the February episode. The QUODDY values are always lower and, apart from the stated extremes, follow NCOM. When discussing these values, one has to bear in mind that observed values as processed may still contain current fluctuations beyond the models' predictive skills. We did calculate the same statistics with an 8th-order, Butterworth, low-pass filter with a cutoff period of 36 hours. Filtering with a longer period predictably lowered the r_O values by

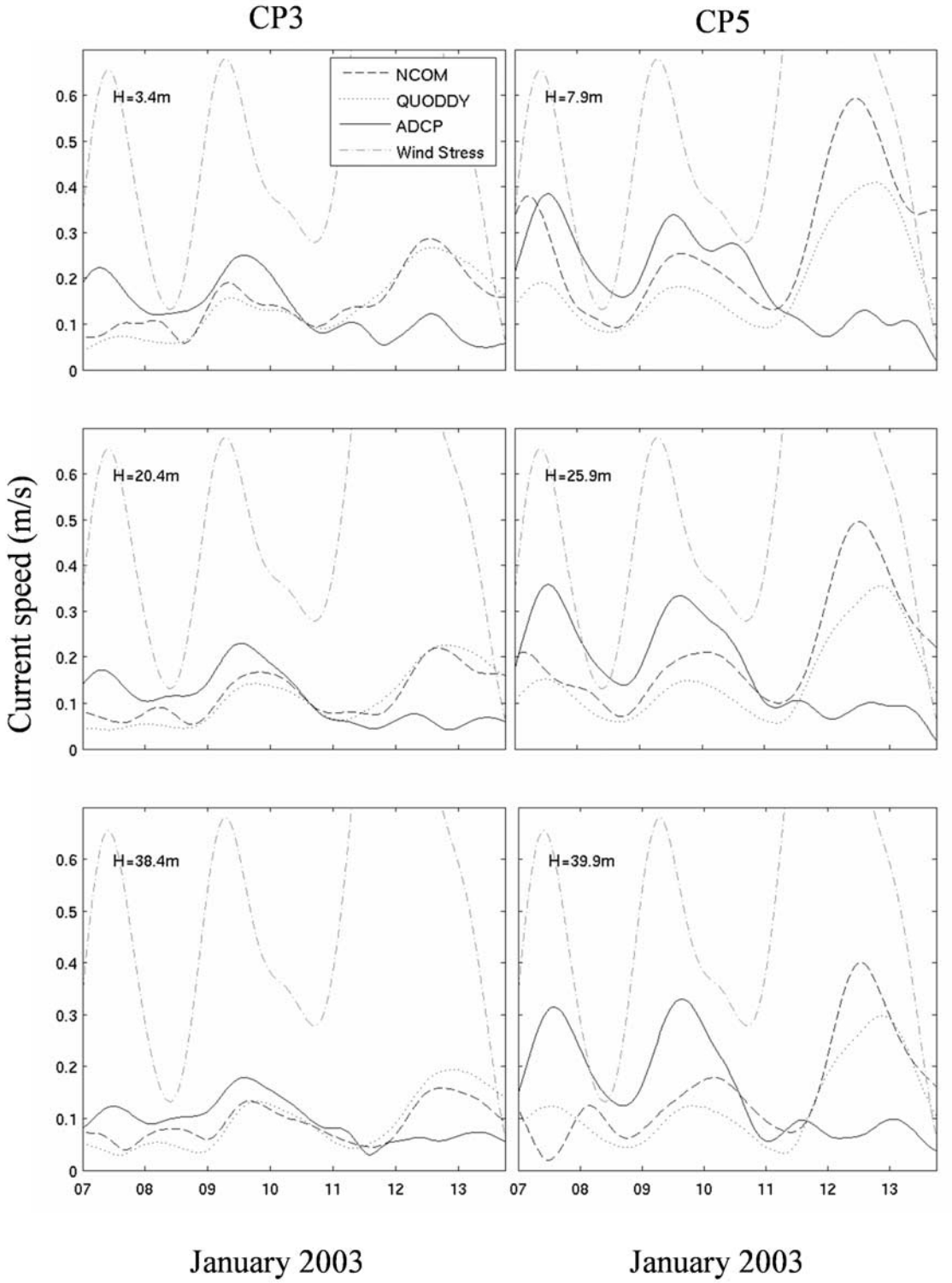

Figure 9. Measured (ADCP) and modeled (NCOM, QUODDY) low-pass-filtered current speed at stations CP3 (left) and CP5 (right) at the depth of the surface (top), middle, and bottom cell location during the January bora episode. Also plotted is the COAMPS wind stress at the Trieste station in N/m^2 scaled by 0.5 to fit the y axis. The x axis denotes days in January.

a few percent, but other statistics did not improve. Also, it is worth reiterating here that the NCOM simulation is a long, seven-month run with momentum, surface heat, and tidal forcing (filtered out before comparison), whereas QUODDY provides only episodic simulations of the wind-forced, barotropic sea. The obtained metric differences invoke discussion of deeper issues beyond the scope of this paper, like deterministic/stochastic nature of the modeled/

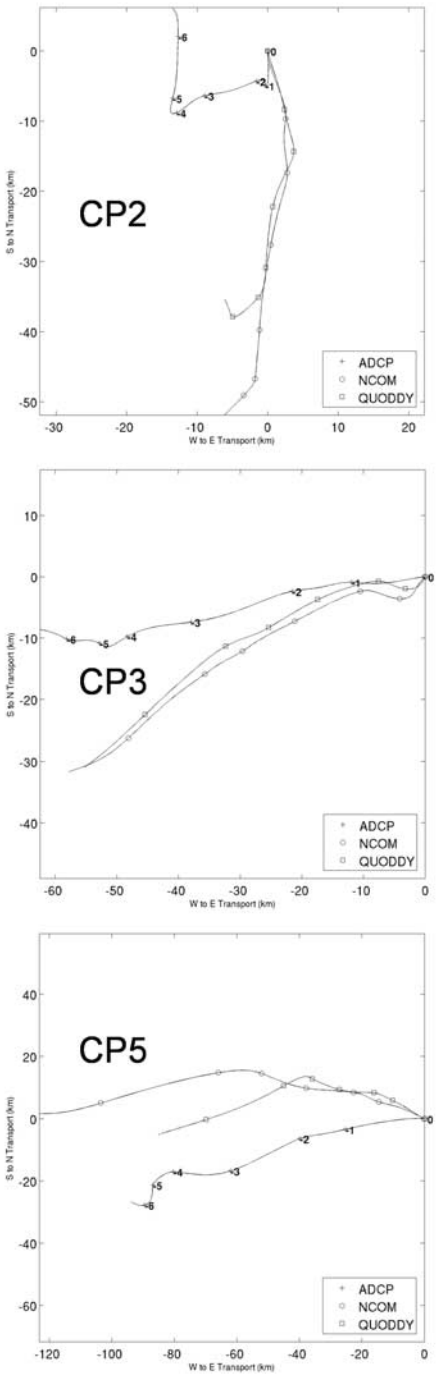

Figure 10. Progressive vector diagrams of the vertically averaged, low-pass-filtered currents at stations CP2, CP3, and CP5 derived from the ADCP measurements (pluses), NCOM model (open circles), and QUODDY model (open squares) for the January bora episode. Numbers denote the number of days since 7 January.

observed variability, or high-resolution model errors at low frequency and/or low wave number scales. In their study of wind quality for oceanographic modeling, *Signell et al.* [2005] derived surface winds from four meteorological models obtaining better model-to-data correlation with coarser model winds. In another study quoted in their paper [*Bogden et al.*, 1996] a 2D wind-forced linear barotropic model outperformed a more realistically forced 3D nonlinear model, based on a model/data misfit metric. One is well advised not to take the obtained NCOM-to-QUODDY differences to represent universal skills of the models in question.

[38] Akin to the data-only analysis presented in Figure 3, the north-south components of both the measured and modeled, vertically integrated and low-pass-filtered velocities at VR1, IC, and CP5 are plotted as scatter diagrams against their east-west counterparts in Figure 11. At VR1, the models for both episodes predict very well a downwind, coast-constrained flow. The polarization is sharper than observed and average speeds are over predicted. At CP5, the data exhibit less polarization and the models to some degree capture that change. The weak response at station IC has proved more difficult to reproduce. In particular, both models mispredict the orientation of the principal variability axis by several tens of degrees. The level of the models' skill in predicting the northern Adriatic response to strong bora events can be still better appreciated by looking at the depth- and episode-averaged flows (Figure 12). The models' responses as well as measurements plotted in the figure were first averaged over the time span of the selected episodes, and then over the local depth. The frictional adjustment time being much shorter than the atmospheric disturbance (KO) assures a swift response and justifies the averaging period. Clearly, both models and both bora events produce the same basic gyral pattern. The observed and modeled flows exhibit high similarity in position, magnitude and direction, but there are some differences. Judging by the VR5 data (see Figure 1) both models appear to underpredict the upwind flow, in February episode in particular. For the January episode both models reproduce somewhat less convincingly the flow direction at the two stations covering the anticyclonic gyre (VR6 and IC) than at VR1 and VR2, but nevertheless model-derived averaged velocities compare well with equally averaged measured values. In all the four averaged fields one notes an area of sluggish currents in which two opposing and bifurcating flows meet: one heading south, reinforcing the Western Adriatic Current (WAC), and the other moving westward, branching off from the Senj gyre northern arm. The location of this area is somewhat different in both models, and for both episodes, always positioned north/northwest of the CP2 station, where measurements indicate very small average current.

[39] To further evaluate the model/data discrepancies in the gyral response, the magnitude of the complex correlation coefficient (ρ) and the angular displacement, or mean directional error, (φ) between the measured (ADCP) and modeled (NCOM, QUODDY) currents were calculated following *Kundu* [1976]:

$$\rho = \frac{\langle u_o u_m + v_o v_m \rangle + i\langle u_o v_m - u_m v_o \rangle}{\sqrt{\langle u_o^2 + v_o^2 \rangle}\cdot\sqrt{\langle u_m^2 + v_m^2 \rangle}} \tag{8}$$

$$\varphi = arctg \frac{\langle u_o v_m - u_m v_o \rangle}{\langle u_o u_m + v_o v_m \rangle} \tag{9}$$

where u and v are, respectively, east-west and north-south, observed (o) or modeled (m), demeaned velocity compo-

Table 3a. Comparative Low-Pass-Filtered Current Statistics: VR1[a]

Period	Depth	r_O	r_N	r_Q	r_{ON}	r_{OQ}	rt_{ON}	rt_{OQ}	rv_{ON}	rv_{OQ}	rm_{ON}	rm_{OQ}
Jan	1.7	.236	.189	.190	1.856	1.540	1.222	.778	2.473	2.182	.835	.346
episode	6.2	.243	.177	.189	1.621	1.439	0.849	.693	1.994	2.096	.482	.244
	14.7	.252	.157	.191	1.350	1.369	0.487	.637	1.350	1.951	.195	.193
	Vbar	.244	.174	.190	1.574	1.417	.799	.677	1.929	2.072	.438	.228
Feb	1.7	.086	.098	.141	1.255	.915	.308	.215	2.926	2.337	.063	.016
episode	6.2	.114	.091	.138	1.145	.879	.273	.235	2.167	1.889	.028	.022
	14.7	.227	.082	.135	1.002	.875	.286	.275	1.254	1.188	.008	.007
	Vbar	.145	.090	.137	1.115	.872	.279	.247	1.975	1.691	.028	.021

[a]Here r_x is the ratio of the time-variant current energy to the total current energy with x equal to O(bserved), N(COM) or Q(UODDY); r_{xy} is the ratio of the root mean square (RMS) of the computed currents to the RMS of the observed currents, rt_{xy} is the ratio of the computed and observed total flow, rv_{xy} is the ratio of the computed and observed time-variable flow, rm_{xy} is the ratio of the computed and observed time-mean flow; the xy equals ON or OQ; vbar marks the column averaged values. The ratio equations are provided in the text; summation is over hourly values within selected period. Depth is in meters.

nents and the brackets represent time averaging. For each model and both time periods, the correlations were computed for each station as a function of depth, starting at the topmost ADCP bin. The complex correlations between the ADCP-observed and NCOM/QUODDY model-predicted currents were typically rather uniform throughout the water column. As a next step, both ρ and φ were further depth averaged to provide one pair of indicators per station and episode. The amplitude correlation results are shown in Figure 13. The best amplitude correlation was obtained for VR5 in January and the worst at VR1 in February. It is clearly related to the fact that, during the January episode, both model predictions closely follow the measured speed at VR5 (Figure 6), whereas, during the February episode at VR1 (not shown), there was a continuous mismatch in speed, with the models first over predicting the observed values and then under predicting them by the end of the episode. As expected from the presented PVDs and scatterplots, both models generated small (10°) average veering at VR1 for the January episode, but larger directional discrepancies at CP5.

6.2. Bora-Driven Extrusion of Coastal Waters

[40] The third issue we wish to explore can be traced back to the *Kuzmić* [1991] paper in which virtual particles and reflectance-derived chlorophyll concentration were used to map the horizontal extent of bora-induced return flow in a simple kinematic framework. Alternatively, the SST can be used to trace bora-induced flow features. We have confined simulations reported in this section to the case of cooling as a source of cold water usable as that kind of tracer.

[41] A flux coupler option was implemented in NCOM to calculate latent and sensible heat fluxes using bulk formulas with NCOM-predicted SST and COAMPS-derived atmospheric fields. The very same heat flux was also used in a related simulation to drive the QUODDY model.

[42] This experiment is focused on the 16–27 February time period when AVHRR scenes were available. Development during this twelve-day sequence is preconditioned in the sense that it follows the strong February bora episode studied in the previous section. In those analyses, however, the thermal aspect was not considered. To address this, we ran an additional QUODDY simulation covering the period 8–16 February since for these terminal dates, relatively clear AVHRR scenes were available for comparison. More specifically, to aid the NCOM output analysis, the QUODDY model was forced, for the same period, with the same NCOM-corrected heat flux starting from a homogeneous, climatologically correct, initial state (T = 8°C, S = 38 psu). The outcome is summarized in Figure 14. The SST difference (16 February–8 February) as obtained with the NCOM model is given in the bottom left corner (Figure 14c), and the same output from the QUODDY model is plotted in the bottom right corner (Figure 14d). The two mentioned AVHRR scenes are also included for reference; one of which covers the beginning (Figure 14a), and the other the end (Figure 14b) of the simulated period. Due to considerable cloudiness on both images (which adds up in the result) differencing of the images was done, but is not presented. Unobstructed parts of the AVHRR difference image suggest a similar situation to that observed in the NCOM and QUODDY difference plots, i.e., a lowering of the average northern Adriatic temperature, a colder strip along the shallow, northwestern coast, and an extruded tongue of colder water. Whereas the NCOM difference is closer to reality (e.g., exhibiting islands of warmer water

Table 3b. Comparative Low-Pass-Filtered Current Statistics: IC[a]

Period	Depth	r_O	r_N	r_Q	r_{ON}	r_{OQ}	rt_{ON}	rt_{OQ}	rv_{ON}	rv_{OQ}	rm_{ON}	rm_{OQ}
Jan	7.2	.264	.669	.681	1.683	.788	4.706	1.108	5.697	0.902	4.351	1.182
episode	19.2	.304	.790	.838	1.280	.688	3.063	0.830	3.440	0.785	2.898	0.850
	39.2	.284	.947	.820	1.155	.750	1.765	0.700	4.938	1.379	0.497	0.428
	vbar	.294	.853	.816	1.259	.717	2.849	0.818	4.145	0.986	2.320	0.751
Feb	7.2	.690	.481	.424	1.614	1.473	3.484	2.305	3.271	2.097	3.956	2.767
episode	19.2	.762	.600	.565	1.158	1.240	2.493	2.134	2.254	1.944	3.257	2.744
	39.2	.560	.595	.673	1.010	1.044	1.246	1.665	1.586	2.313	0.813	0.839
	vbar	.694	.566	.589	1.167	1.202	2.265	2.007	2.136	2.059	2.703	2.109

[a]As in Table 3a.

Table 3c. Comparative Low-Pass-Filtered Current Statistics: CP5[a]

Period	Depth	r_O	r_N	r_Q	r_{ON}	r_{OQ}	rt_{ON}	rt_{OQ}	rv_{ON}	rv_{OQ}	rm_{ON}	rm_{OQ}
Jan	7.9	.294	.259	.305	1.399	.983	1.271	.813	3.651	2.666	.278	.041
episode	21.9	.316	.273	.344	1.233	.898	1.099	.800	3.111	2.421	.170	.052
	39.9	.339	.334	.381	1.003	.804	1.038	.768	2.832	2.080	.119	.096
	vbar	.322	.285	.349	1.199	.879	1.100	.787	3.100	2.336	.167	.062
Feb	7.9	.223	.239	.316	1.854	1.155	1.194	.372	2.735	1.476	.752	.055
episode	21.9	.232	.276	.350	1.628	1.010	0.801	.329	2.200	1.264	.379	.047
	39.9	.238	.388	.380	1.270	0.848	0.491	.392	1.853	1.269	.066	.119
	vbar	.236	.295	.354	1.576	0.983	0.774	.350	2.144	1.269	.354	.067

[a]As in Table 3a.

advected from the south) the QUODDY difference is perhaps more instructive. The 2.5–3.0°C temperature drop observed in the plot clearly traces the extent of both the Trieste and Senj gyres. It is important to stress here that the Po River was not included in the QUODDY simulation either as a flow/velocity or temperature boundary condition. Therefore, the tongue of extruded colder water seen in the QUODDY differential image is the sea water cooled along

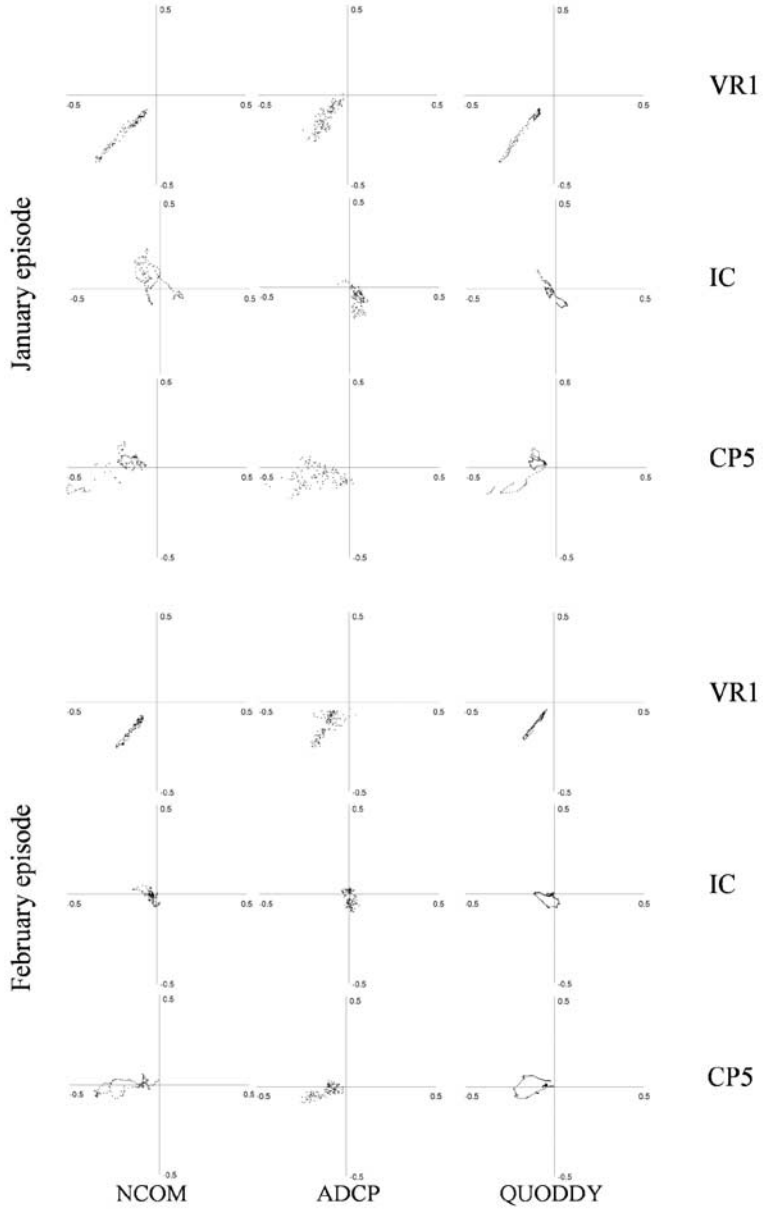

Figure 11. Scatterplot of the vertically averaged currents at the VR1, IC, and CP5 stations: modeled with NCOM (left), ADCP-measured (middle), and modeled with QUODDY (right) during the January (top) and February (bottom) bora episodes.

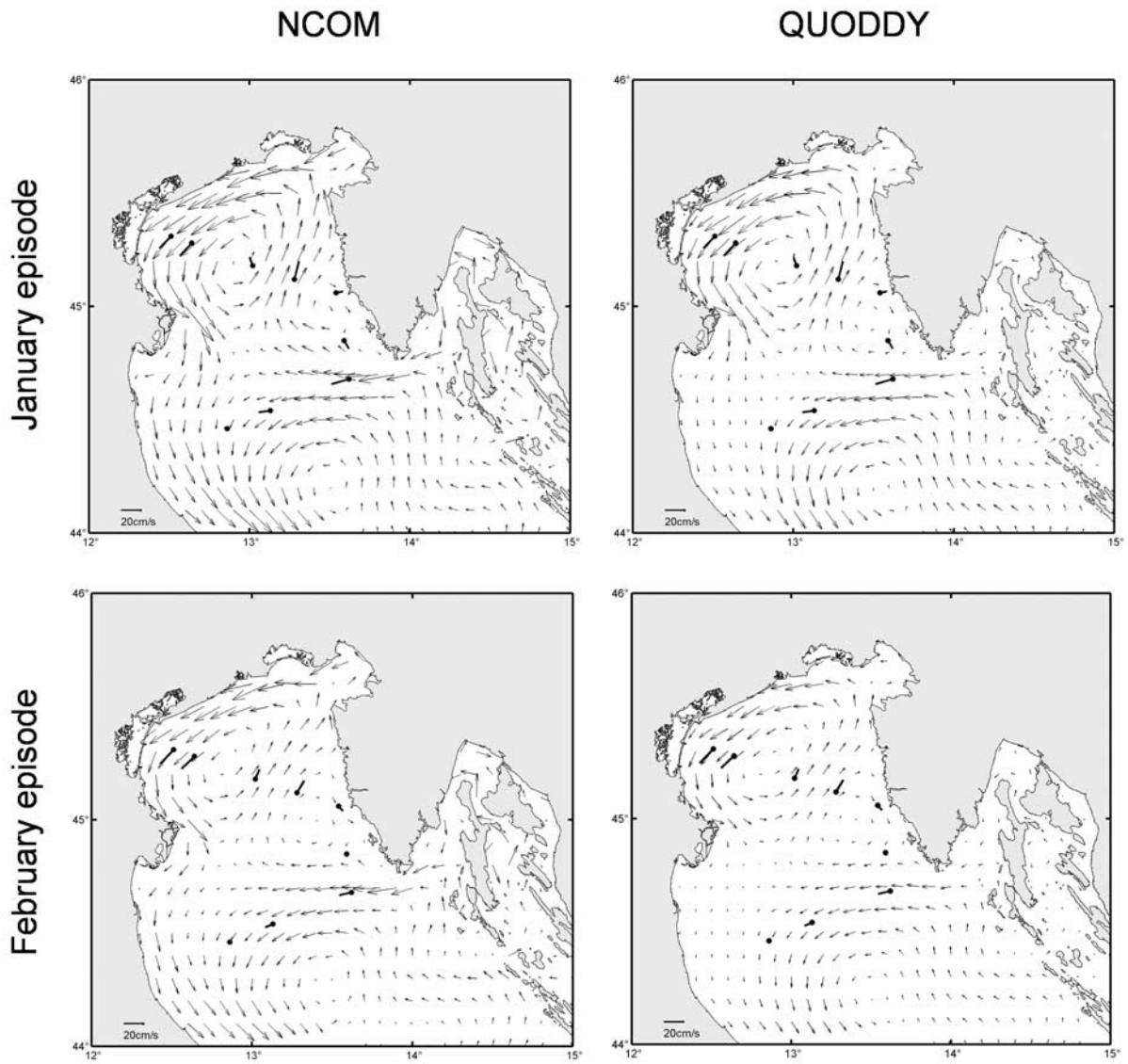

Figure 12. Depth and episode averaged flow computed with the two models and measured at nine stations. Thick vectors, with dots at their roots, mark the averaged measured currents. The NCOM output is rotated to the northeast grid and resampled with 0.1° resolution. The unstructured-mesh QUODDY output is mapped onto the same grid. The time averaging periods equal the duration of the selected bora episodes.

the shallow, northwestern, coastal strip and spun up offshore by the bora wind. Another cold-water tongue is obtained further south tracing the northern arm of the Senj gyre. This cooling, traceable as well in the AVHRR scenes in Figure 14, entails intensification of the meridional gradient in the area south of the Istrian peninsula, a result also obtained by B. Cushman-Roisin and K. A. Korotenko (Mesoscale-resolving simulations of summer and winter bora events in the Adriatic Sea, submitted to *Journal of Geophysical Research*, 2006) in their mesoscale-resolving simulation of the winter bora (11–20 February 2003).

[43] The 16–27 February simulation was done only with the NCOM model (because it included the thermal fluxes at the air-sea interface). The AVHRR data and this simulation outcome are presented in Figures 15 and 16, respectively. The NCOM simulation of the northern Adriatic SST over the twelve-day period (Figure 16) is to be compared to the same sequence derived from the AVHRR observations (Figure 15). The same palette is applied in both sequences. On top of each figure, the wind magnitude measured at Trieste station is plotted to aid the analysis. The stars on the plot mark the slightly variable, midday times when the AVHRR scenes were acquired and the vertical bars mark the noon of each day for which NCOM predictions were calculated. Although the AVHRR scenes are contaminated with clouds, both sequences clearly exhibit a meridional temperature difference and a frontal zone approximately following the 50-m bathymetry line. This frontal zone separates the shallower north, which is impacted by fresh-water runoff and more pronounced cooling, from the deeper

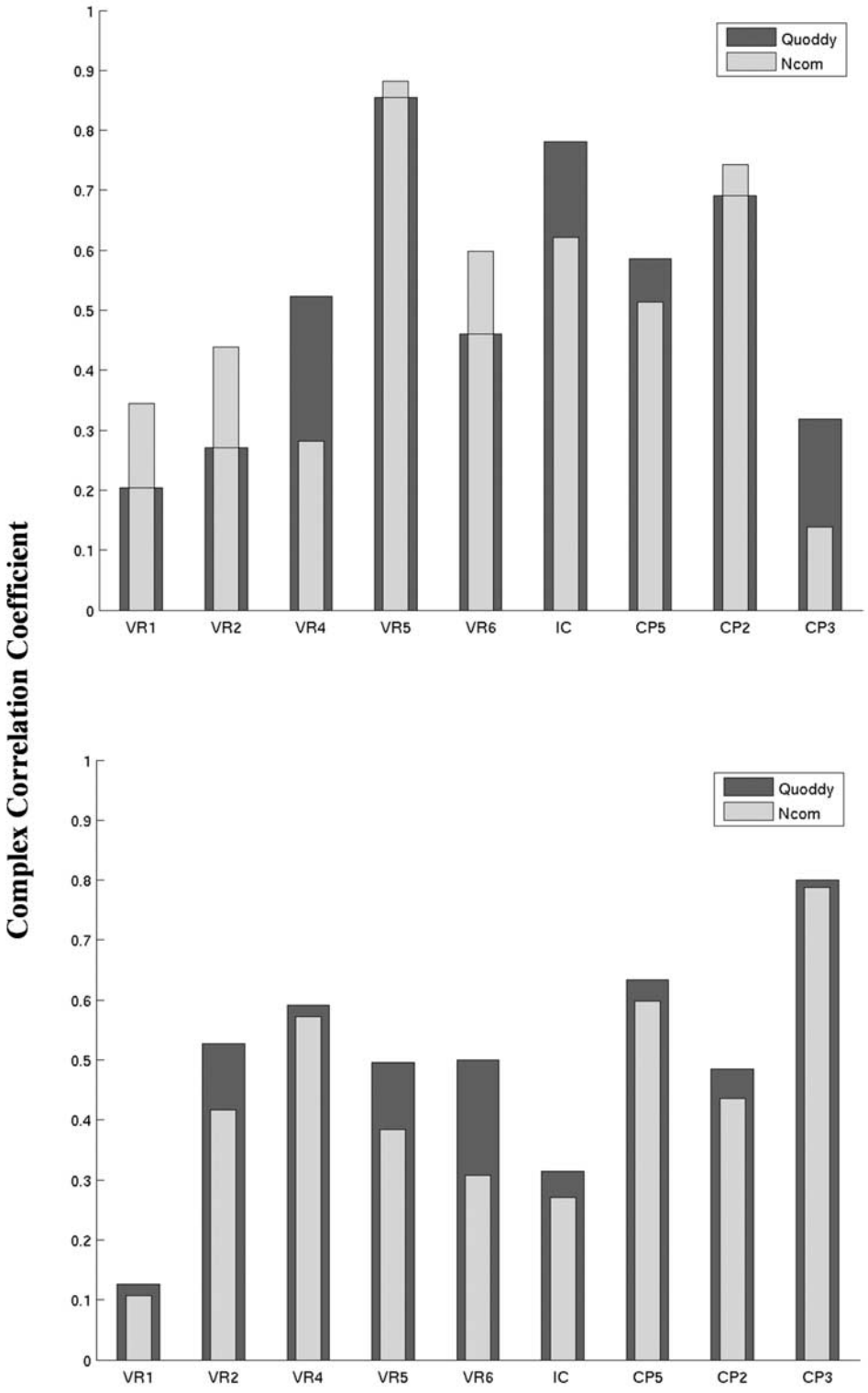

Figure 13. Vertically averaged magnitudes of the complex correlation between the low-pass-filtered model-predicted (NCOM, QUODDY) and observed currents at nine stations during the January (top) and February (bottom) bora episodes.

south, which is influenced by advection of warmer and saltier waters. *Zore-Armanda and Gačić* [1987] related the position of this thermal front to the frequency of the bora wind.

[44] In Figure 15 one notes on 16 and 17 February accumulation of colder water south of the Po delta; the water is both discharged by the Po River and advected there alongshore by the Trieste gyre. The bulge appears colder

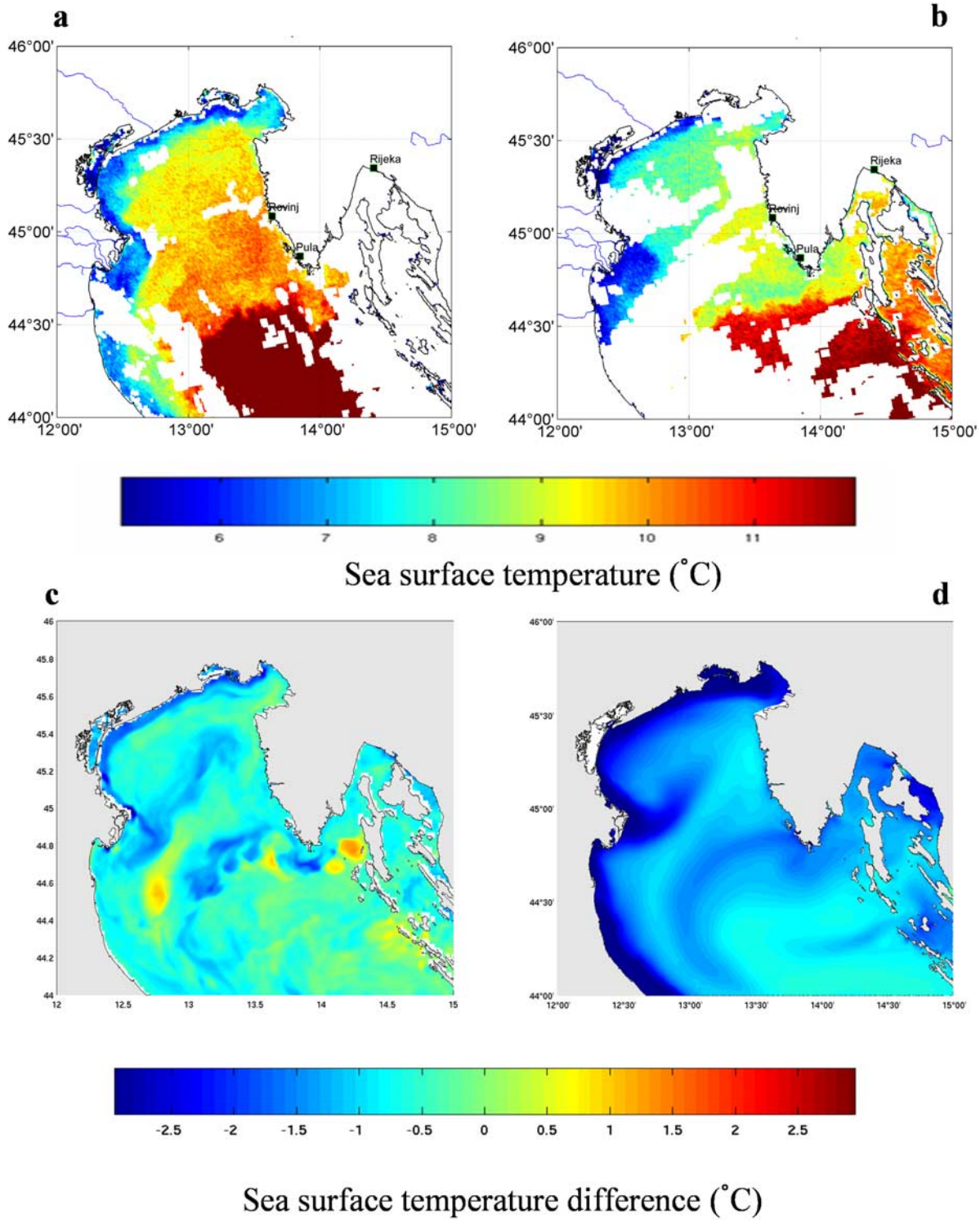

Figure 14. Sea surface temperature observed with the AVHRR sensor on (a) 8 February 2003 and (b) 16 February 2003. The plots at the bottom show the related sea surface temperature difference (16.02.2003–08.02.2003) as calculated with the (c) NCOM and (d) QUODDY models.

(and closer to the 4.2°C and 3.5°C temperature values measured on 16 and 17 February, respectively, at a Po upstream location–J. Chiggiato, personal communication) in the AVHRR scenes than in the NCOM simulations. The difference should be partly ascribed to the fact that no actual river temperatures were used as a Po River boundary condition in the NCOM simulation (Adriatic monthly climatological values were used instead). Consequently, one can see on most of the images in Figure 16 tiny islands of anomalously higher-temperature water at the locations of

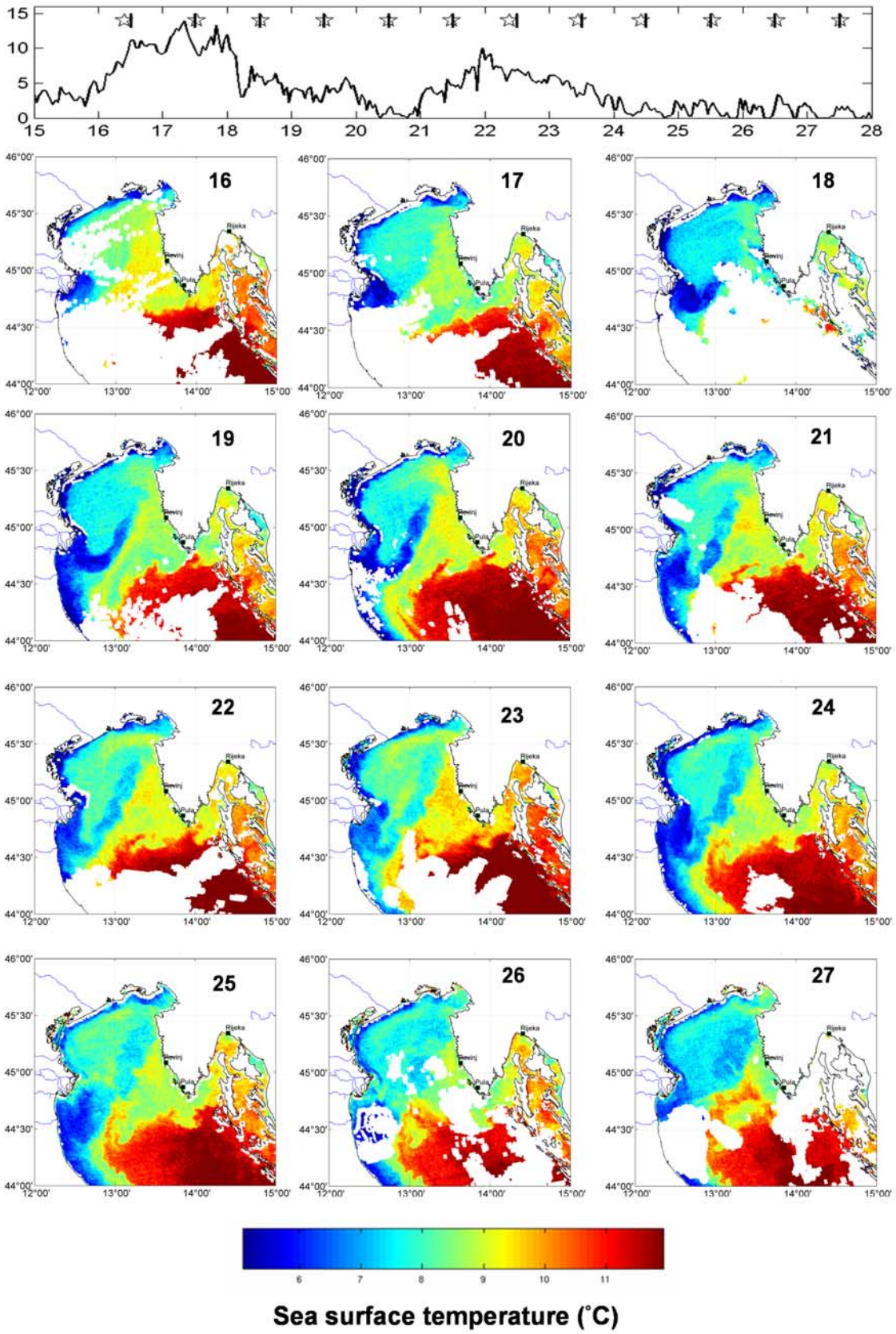

Figure 15. Sea surface temperature during the period 16–27 February 2003 as observed with the AVHRR sensor. Plotted at the top is the wind magnitude measured at the Trieste station. Stars mark the times of the AVHRR scenes, and vertical bars mark the times of the corresponding SST fields as predicted with the NCOM model.

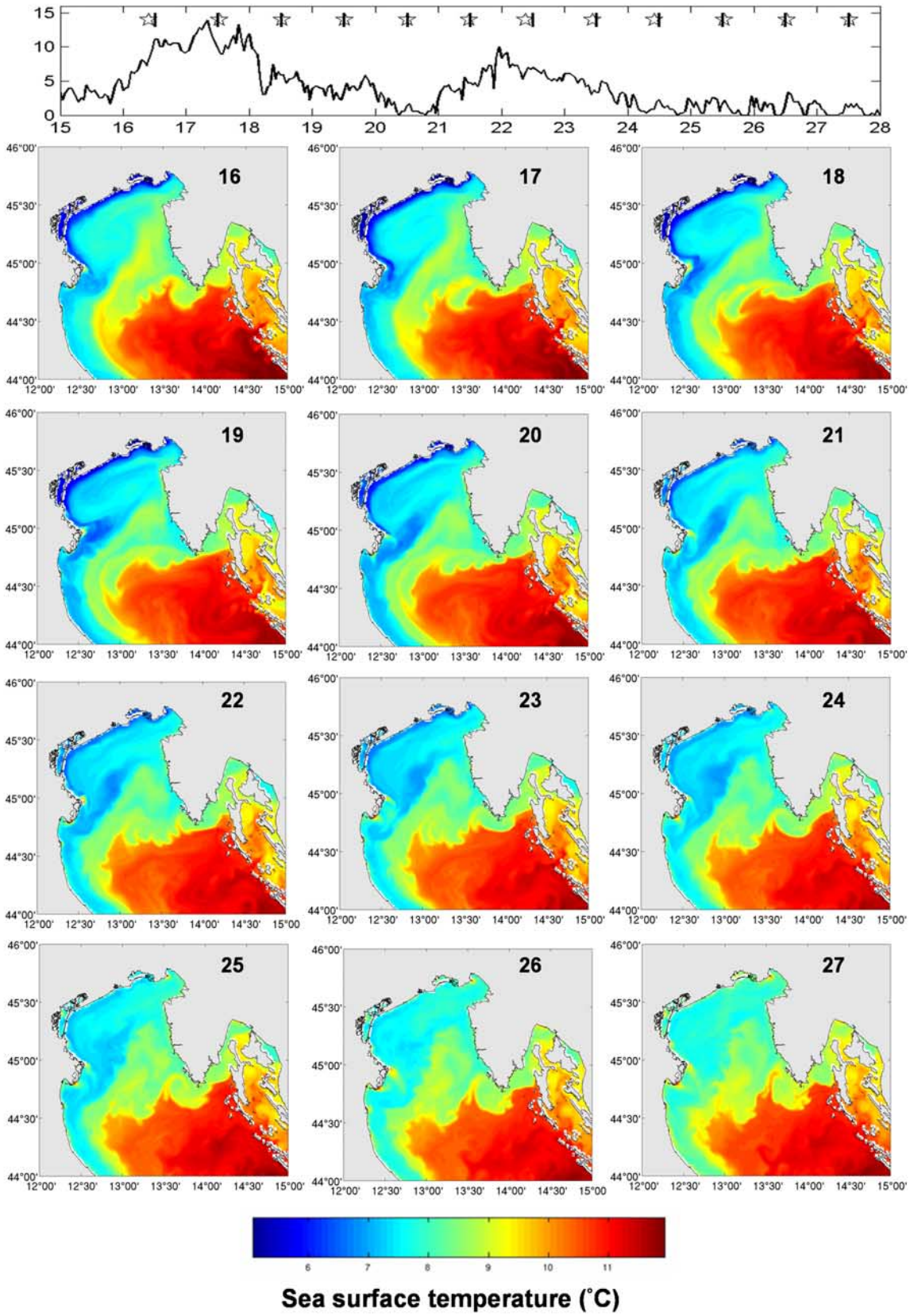

Figure 16. Sea surface temperature during the period 16–27 February 2003 as predicted with the NCOM model. Plotted at the top is the wind magnitude measured at the Trieste station. Vertical bars mark the times of the model-predicted SST fields, and stars mark the registration times of the corresponding AVHRR scenes.

the Po River outflow. One should bear in mind that this sequence also exhibits the remnants of the previously spun up colder water visible in both the remotely sensed image and the NCOM simulation for 16 February. The model appears to predict a sharper than observed frontal gradient around 9°C. Although clouds obstruct the view of the northwestern shallow strip throughout most of the sequence, closer inspection reveals fairly well the correspondence between the modeled and observed SST. On the background of the previous thermal signature, one observes the extrusion of new cold water spun up by the two-day bora event, which, after a break of about a day and a half, followed our February episode. The extrusion can be traced in both the observed and simulated sequences. *Kuzmić* [1991] exploited a circumstance that these waters under riverine influence (the Po River in particular) are also highly turbid and therefore also observable by optical sensors (CZCS). Present-day sensors are even more useable in that regard, as the Figure 1.4 in *Lee et al.* [2005b], for example, clearly testifies. The reported SeaWiFS image registered on 23 February 2003 maps out a chlorophyll concentration pattern very similar to the SST pattern presented in Figure 15. With the bora subsiding over the following days, subsequent images of the cold water tongue exhibit instabilities and meandering (more pronounced in the AVHRR images than in the NCOM simulation) and eventual dissolution of the temperature tongue. Throughout this period, one can trace in the frontal zone on the southern boundary of the basin the creation and destruction of warm water filaments. A series observed over a week-long period (21–27 February) in the AVHRR scenes appears to trace development of a filament controlled by a clockwise motion. The same series is visible but less pronounced in the NCOM sequence, which, over a somewhat shorter period (24–27 February), shows the development of a similar filament closer to the tip of Istria and the Rovinj anticyclonic gyre.

7. Summary and Conclusions

[45] A combination of recent intensive observations and simulations with two numerical models was used to revisit the issue of the northern Adriatic response to strong bora episodes. The simplistic simulations reported in the KO paper have been reconsidered in the light of recent field evidence and more insightful modeling results. This new information is summarized in Figure 17b, in a manner convenient for synthesis, and comparison with previous results. Both new observed and simulated data reinforce the KO finding that an episode of strong bora wind provokes a double-gyre (cyclonic, Trieste, and anticyclonic, Rovinj) response of the northern Adriatic north of the Po Delta - Pula line (Figure 17b). The old KO simulations, based on a linear model and steady climatological wind forcing, successfully predicted the mechanistic, barotropic nature of the induced gyral pattern and the appearance of an upwind return flow between the counter-rotating gyres (Figure 17a). New modeling solutions, driven by higher-resolution, time-variant wind, position the Trieste cyclonic gyre predominantly north of the Po Delta–Rovinj line, in good agreement with new empirical evidence along the gyre's northeastern (NE) and northestern (NW) arms (area 1 in Figure 17b). The gyre's NW arm is geometrically constrained by the northwestern Adriatic coast and intensified by the shallowness of the coastal zone. During an intense bora episode, both the measured and modeled statistics picture a downwind, highly polarized ($\varepsilon \leq 0.18$), and almost depth-independent ($\gamma \geq 0.93$) flow within the arm. The other (NE) arm maintains a sharp polarization and high depth dependence while exhibiting lower speed, with both models again in good accord with observations. Although there were no ADCP measurements in the gyre's southern

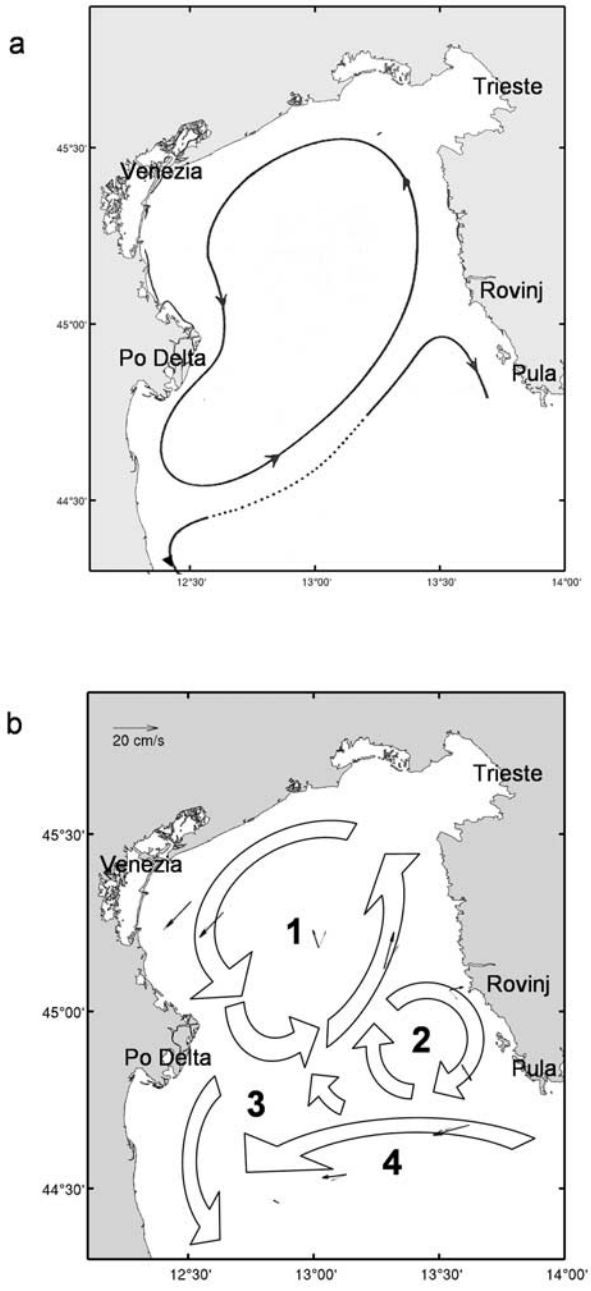

Figure 17. Schematic of the bora-induced circulation in the northern Adriatic: (a) as reported in the KO paper; (b) as derived in the present work. The numbers in Figure 17b mark the four characteristic bora-response areas discussed in the text. Also plotted in Figure 17b are the depth- and episode-averaged currents; thick vectors, January episode; thin vectors, February episode.

section, water movements deducible from a sequence of AVHRR SST scenes reinforce the model solutions.

[46] Both the simulations and measurements place the other, Rovinj gyre (area 2 in Figure 17b) off the west Istrian coast, with no comparable field information across the basin, and closer to the other shore. The current statistics for the Rovinj gyre provide lower maximum and average-speed values and less polarized ($\varepsilon \leq 0.54$) but still rather depth independent ($\gamma \geq 0.94$) flow, while predicting a clockwise rotation. Apart from some directional discrepancies, the gyre is clearly in accord with measurements. South of the Po Delta - Pula line (area 3), both models predict a southward flow contributing to the WAC, and an area of sluggish flow between this southward flow, and a flow branching from the Senj gyre northern arm. The northern (upper) arm of the Senj cyclonic gyre, observed and model-generated in area 4 was not properly resolved in the KO model, due to the closeness of their open boundary. In contrast to the Trieste gyre, the Senj gyre northern arm is unconstrained geometrically, enjoying more lateral freedom and exhibiting less rectilinear ($\varepsilon \leq 0.42$) flow.

[47] This multigyral response is a prominent generic, albeit transient, feature of the northern Adriatic flow, imbedded in cyclonic general circulation. As several previous modeling (e.g., KO) and field [e.g., *Hopkins et al.*, 1999] studies have established, the bora generates convergence against and sea-level rise toward the western boundary, which sustains a cyclonic flow. The easterly jets of both the Trieste and Senj bora induce flows that also feed the WAC. Due to orographic incisions in the Dinaric Alps, the bora exhibits strong horizontal vorticity (wind stress curl), which is responsible for imposing the observed gyral pattern, entailing high-resolution requirements on the wind forcing field. Our literature review reinforces the notion that the modeling studies based on coarser ECMWF wind fields fail to capture the smaller-scale vorticity and related response pattern. But even when the basic response pattern is captured correctly, still finer resolution is likely to be required to resolve the important details. As the sea-response circulation pattern is tightly coupled with the forcing wind field, any weakness in wind simulation is promptly reflected in the modeled sea response.

[48] The COAMPS model successfully simulated the onset, duration, and decay of the wind peaks in studied bora episodes, exhibiting a tendency to overpredict the strength of the bora in the northern Adriatic. Bora structures that are apparently driven by topography on a scale finer than resolved by COAMPS (4 km) are not well represented in the simulated winds, so improved orography representation may improve its wind field predictions. Further improvement may come from coupling to a wave model, since feedback of wave-induced stress might reduce or eliminate the wind speed overprediction observed in analyzed bora episodes. Using a coupled atmosphere-ocean wave model, *Doyle* [2002] found reduction of predicted wind speeds in excess of 10 ms^{-1} when simulating tropical cyclones and a bora event.

[49] The bora events are also characterized by pronounced cooling and heat loss to the atmosphere, but neither JRP nor WISE had a component to adequately address this aspect of the bora. Our NCOM and QUODDY simulations were therefore focused on cooling as a source of cold water usable as a tracer of bora-induced flow features. The modeling results have identified the shallow NW coastal strip as an important source of the colder water observed in a sequence of remotely sensed SST fields derived from AVHRR data. A comparison with a related sequence of NCOM-generated SST fields provided good semi-quantitative agreement.

[50] With ADCP-registered current time-series in excess of 200 days, about 10 wave and tide-gauge records, 5 coastal wind data time series, and at least as many related series generated by the atmospheric and two oceanic models, there is great potential for frequency domain analysis. Cross and cospectral analyses of those data sets should reveal valuable information about coherence, energetics, and phase relationships among the involved variables, shedding further light on the intricacies of the bora-driven flows. This task is already started and we plan to submit a comprehensive report in a separate paper.

[51] **Acknowledgments.** Fabio Raicic (IT, Trieste) kindly provided the Trieste wind data, and Robert Precali (RBI/CMR, Rovinj) put at our disposal the Rovinj wind data. We are grateful to the Croatian Meteorological and Hydrological Service for the Mali Lošinj, Pula, and Senj wind data. James D. Doyle was supported by the Office of Naval Research's Program Element 0601153N, with computing time supported in part by a grant of HPC time from the Department of Defense Major Shared Resource Center, Aberdeen, Maryland. The work of Jeffrey W. Book and Paul J. Martin was supported by the Office of Naval Research as part of the research programs "Adriatic Circulation Experiment" and "Dynamics of the Adriatic in Real-Time" under Program Element 0602435N. Milivoj Kuzmić and Ivica Janeković were supported by the Croatian Ministry of Science, Education, and Sport via research grant 0098113. The WISE Experiment was funded by the Jadran Project. Insightful comments of two anonymous reviewers helped improve the manuscript. The AVHRR images were created with a graphic interface designed and programmed by Igor Tomažić. A modified vecDiagram Matlab function from Dave Jones Fathom Toolbox was used to create the PVDs. COAMPS is a registered trademark of the Naval Research Laboratory.

References

Barron, C. N., A. B. Kara, P. J. Martin, R. C. Rhodes, and L. F. Smedstad (2005), Formulation, implementation and examination of vertical coordinate choices in the global Navy Coastal Ocean Model (NCOM), *Ocean Modell.*, doi:10.1016/j.ocemod.2005.01.004.

Beg Paklar, G., V. Isakov, D. Koračin, V. Kourafalou, and M. Orlić (2001), A case study of bora-driven flow and density changes on the Adriatic Shelf (January 1987), *Cont. Shelf Res.*, *21*, 1752–1783.

Bergamasco, A., and M. Gačić (1996), Baroclinic response of the Adriatic Sea to an episode of Bora wind, *J. Phys. Oceanogr.*, *26*, 1354–1369.

Blumberg, A. F., and G. L. Mellor (1987), A description of a three-dimensional coastal ocean circulation model, in *Three-Dimensional Coastal Ocean Models*, edited by N. Heaps, AGU, Washington, D. C.

Bogden, P. S., P. Malanotte-Rizzoli, and R. Signell (1996), Open-ocean boundary conditions from interior data: Local and remote forcing of Massachusetts Bay, *J. Geophys. Res.*, *101*, 6487–6500.

Csanady, G. T. (1975), Hydrodynamics of the large lakes, *Ann. Rev. Fluid Mech.*, *7*, 357–386.

Cushman-Roisin, B., M. Gačić, P.-M. Poulain, and A. Artegiani (Eds.) (2001), *Physical Oceanography of the Adriatic Sea: Past, Present and Future*, 304 pp., Springer, New York.

Dorman, C. E., et al. (2006), February 2003 marine atmospheric conditions and the bora over the northern Adriatic Sea, *J. Geophys. Res.*, doi:10.1029/2005JC003134, in press.

Doyle, J. D. (2002), Coupled atmosphere-ocean wave simulations under high wind conditions, *Mon. Weather Rev.*, *130*, 3087–3099.

Egbert, G. D., and S. Y. Erofeeva (2002), Efficient inverse modeling of barotropic ocean tides, *J. Atmos. Oceanic Technol.*, *19*, 183–204.

Emery, W. J., and R. E. Thompson (1997), *Data Analysis Methods in Physical Oceanography*, 634 pp., Elsevier, New York.

Franco, P., and A. Michelato (1992), Northern Adriatic Sea: Oceanography of the basin proper and of the western coastal zone, *Sci. Total Environ.*, suppl., 35–62.

Galperin, B., L. H. Kantha, S. Hassid, and A. Rosati (1988), A quasi-equilibrium turbulent energy model for geophysical flows, *J. Atmos. Sci.*, *45*, 55–62.

Hodur, R. M. (1997), The Naval Research Laboratory's Coupled Ocean/Atmosphere Mesoscale Prediction System (COAMPS), *Mon. Weather Rev.*, *125*, 1414–1430.

Holland, W. R., J. C. Chow, and F. O. Bryan (1998), Application of a third-order upwind scheme in the NCAR Ocean Model, *J. Clim.*, *11*, 1487–1493.

Hopkins, T. S., A. Artegiani, C. Kinder, and R. Pariante (1999), A discussion of the northern Adriatic circulation and flushing as determined from the ELNA hydrography, in *The Adriatic Sea*, *Ecosyst. Res. Rep. 32*, pp. 85–106, Off. for Off. Publ. of the Eur. Commun., Luxembourg.

Ivančan-Picek, B., and V. Tutiš (1996), A case study of severe Adriatic bora on 28 December 1992, *Tellus, Ser. A*, *48*, 357–367.

Janeković, I., and M. Kuzmić (2005), Numerical simulation of the Adriatic Sea principal tidal constituents, *Ann. Geophys.*, *23*, 3207–3218.

Janeković, I., M. Kuzmić, J. W. Book, and H. T. Perkins (2004), A tidal model of the Adriatic Sea: ACE/WISE contribution to its current response validation, paper presented at Venice Adriatic Workshop, Off. of Nav. Res. Global, Venice, Italy, 14–16 June.

Kara, A. B., C. N. Barron, P. J. Martin, L. F. Smedstad, and R. C. Rhodes (2005), Validation of interannual simulations from the 1/8 Global Navy Coastal Ocean Model (NCOM), *Ocean Modell.*, doi:10.1016/j.ocemod.2005.01.003.

Kondo, J. (1975), Air-sea bulk transfer coefficients in diabatic conditions, *Boundary Layer Meteorol.*, *9*, 91–112.

Kundu, P. K. (1976), Ekman veering observed near the ocean bottom, *J. Phys. Oceanogr.*, *6*, 238–242.

Kuzmić, M. (1991), Exploring the effects of bora over the northern Adriatic: CZCS imagery and a mathematical model prediction, *Int. J. Remote Sens.*, *12*, 207–214.

Kuzmić, M., and M. Orlić (1987), Wind-induced vertical shearing: ALPEX/MEDALPEX data and modelling exercise, *Ann. Geophys.*, *5B*, 103–112.

Kuzmić, M., M. Orlić, and Z. Pasarić (1988), Mathematical modelling (in Croatian), in *1987 Annual Report*, edited by R. Precali and Z. Konrad, chap. 5, pp. 331–352, Joint Yugoslav-Italian Sci. Coop. Program, Rovinj, Croatia.

Large, W. G., and S. Pond (1981), Open ocean momentum flux measurements in moderate to strong winds, *J. Phys. Oceanogr.*, *11*, 324–336.

Lazić, L., and I. Tošić (1998), A real data simulation of the Adriatic Bora and the impact of mountain height on the Bora trajectories, *Meteorol. Atmos. Phys.*, *66*, 143–155.

Lee, C., et al. (2005a), Northern Adriatic response to a wintertime bora wind event, *Eos Trans. AGU*, *86*(16), 157–168.

Lee, C., et al. (2005b), Cruise report: DOLCE VITA 1 and 2, 31 January–23 February and 26 May–15 June, 2003, *Tech. Rep., APL-UW TR 0409*.

Loglisci, N., M. W. Qian, N. Rachev, C. Cassardo, A. Longhetto, R. Purini, P. Trivero, S. Ferrarese, and C. Giraud (2004), Development of an atmosphere-ocean coupled model and its application over the Adriatic Sea during a severe weather event of Bora wind, *J. Geophys. Res.*, *109*, D01102, doi:10.1029/2003JD003956.

Lynch, D. R., and F. E. Werner (1991), Three-dimensional hydrodynamics on finite elements. Part II: Non-linear time-stepping model, *Int. J. Numer. Methods Fluids*, *12*, 507–533.

Lynch, D. R., T. C. I. Justin, C. E. Naimie, and F. E. Werner (1996), Comprehensive coastal circulation model with application to the Gulf of Maine, *Cont. Shelf Res.*, *16*, 875–906.

Martin, P. J. (2000), A description of the Navy Coastal Ocean Model Version 1.0, *NRL Rep. NRL/FR/7322-00-9962*, 42 pp., Nav. Res. Lab., Stennis Space Cent., Miss.

Mellor, G. L. (1991), An equation of state for numerical models of oceans and estuaries, *J. Atmos. Oceanic Technol.*, *8*, 609–611.

Mellor, G. L., and T. Yamada (1974), A hierarchy of turbulence closure models for planetary boundary layers, *J. Atmos. Sci.*, *31*, 1791–1806.

Mellor, G. L., and T. Yamada (1982), Development of a turbulence closure model for geophysical fluid problems, *Rev. Geophys.*, *20*, 851–875.

Morey, S. L., P. J. Martin, J. J. O'Brien, A. A. Wallcraft, and J. Zavala-Hidalgo (2003), Export pathways for river discharged fresh water in the northern Gulf of Mexico, *J. Geophys. Res.*, *108*(C10), 3303, doi:10.1029/2002JC001674.

Orlić, M., M. Kuzmić, and Z. Pasarić (1994), Response of the Adriatic Sea to the bora and sirocco forcing, *Cont. Shelf Res.*, *14*, 91–116.

Penzar, B. (1977), Air pressure–wind (in Croatian), *Prilozi poznavanju vremena i klime*, *2*, 117 pp.

Perkins, H. T., F. de Strobel, and L. Gualdesi (2000), The Barney Sentinel Trawl-resistant ADCP bottom mount: Design, testing, and application, *IEEE J. Oceanic Eng.*, *25*, 430–436.

Poulain, P.-M., V. H. Kourafalou, and B. Cushman-Roisin (2001), Northern Adriatic Sea, in *Physical Oceanography of the Adriatic Sea: Past, Present and Future*, chap. 5, edited by B. Cushman-Roisin et al., pp. 143–165, Springer, New York.

Pullen, J., J. D. Doyle, R. Hodur, A. Ogston, J. W. Book, H. Perkins, and R. Signell (2003), Coupled ocean-atmosphere nested modeling of the Adriatic Sea during winter and spring 2001, *J. Geophys. Res.*, *108*(C10), 3320, doi:10.1029/2003JC001780.

Rachev, N., and R. Purini (2001), The Adriatic response to the bora forcing: A numerical study, *Nuovo Cimento*, *24C*, 303–311.

Raicich, R. (1994), Note on the flow rates of the Adriatic rivers, *Tech. Rep. RF 02/94*, 8 pp., Cons. Naz. delle Ric. Inst. Sper. Talassografico, Trieste, Italy.

Schwab, D. J., A. H. Clites, C. R. Murthy, J. E. Sandwell, L. A. Meadows, and G. M. Meadows (1989), The effect of wind on transport and circulation in Lake St. Clair, *J. Geophys. Res.*, *94*, 4947–4958.

Schwing, F. B., L.-Y. Oey, and J. O. Blanton (1985), Frictional response of continental shelf waters to local wind forcing, *J. Phys. Oceanogr.*, *15*, 1733–1746.

Shtokman, V. B. (1941), Vetrovoi nagon i gorizontalynaya cirkulaciya v zamknutom morye nebolshoy glubiny (in Russian), *Izv. AN SSSR, Ser. Geograficheskaya i geofizicheskaya*.

Signell, R. P., S. Carniel, L. Cavaleri, J. Chiggiato, J. D. Doyle, J. Pullen, and M. Sclavo (2005), Assessment of wind quality for oceanographic modelling in semi-enclosed seas, *J. Mar. Syst.*, *53*, 217–233.

Smagorinsky, J. (1963), General circulation experiments with the primitive equations I. The basic experiment, *Mon. Weather Rev.*, *91*, 99–164.

Spoler-Canić, K., and L. Kraljević (2005), The impact of model resolution on simulated distribution of bura, *Croat. Meteorol. J.*, *40*, 296–299.

Stravisi, F. (1977), Bora driven circulation in the northern Adriatic, *Boll. Geofis. Teor. Appl.*, *19*, 95–102.

Thompson, K. R., and D. T. Pugh (1986), The subtidal behaviour of the Celtic Sea–II. Currents, *Cont. Shelf Res.*, *5*, 321–346.

Wang, X. H. (2005), Circulation and heat budget of the northern Adriatic Sea (Italy) due to a Bora event in January 2001: A numerical model study, *Ocean Modell.*, *10*, 253–271.

Yoshino, M. (1972), Monthly mean wind frequency and force by directions at selected climatological stations in Yugoslavia, *Climatol. Notes*, *10*, 23–44.

Yoshino, M. (1976), *Local Wind Bora*, 289 pp., Univ. of Tokyo Press, Tokyo, Japan.

Zore-Armanda, M., and M. Gačić (1987), Effects of bora on the circulation in the North Adriatic, *Ann. Geophys.*, *5B*, 93–102.

J. W. Book and P. J. Martin, Oceanography Division, Naval Research Laboratory, Stennis Space Center, MS 39529-1105, USA.

J. D. Doyle, Marine Meteorology Division, Naval Research Laboratory, Monterey, CA 93943, USA.

I. Janeković and M. Kuzmić, Center for Marine and Environmental Research, Ruđer Bošković Institute, P.O. Box 180, 10002 Zagreb, Croatia. (kuzmic@rudjer.irb.hr)